Service Providers: Jeffrey Cornwell, Larry Sanford and Michael Owens
Scope Number: 12 – Cost Effective Denitrification in Oyster Reefs

Final Report – August 2022

Award 19255

UMCES Contribution TS-784-22

Table of Contents

List of Tables 3
List of Figures 3
Introduction 6
Background 6
Need for a New Approach 6
Approach Overview 7
Methods 8
Chamber Construction 8
Mixing Experiments 10
Field Deployments 12
Sites and Characteristics 12
Deployment Protocol 14
Sample Collection and Analysis 17
Calculations 18
Results and Discussion 22
Operational Observations 22
Leakage Estimates 22
Oxygen Time Courses and Fluxes 25
Nutrient Fluxes and Denitrification 25
Ammonium Fluxes 26
Nitrate + Nitrite (NO_x^-) Fluxes 29
Di-Nitrogen (N_2) Fluxes 31
Little Choptank Denitrification and Nitrogen Fluxes 36
Potential Improvements to Design and Operation 39
Acknowledgments 42
References 42
Appendix I. Materials List 44
Appendix II. Cost Estimates For Denitrification 45

List of Tables

Table 1. Lander deployments. Note that replicates were done on 8/25 and 9/17, with two sites within 10 m of each other. 13
Table 2. Site characteristics from 4 sites used for testing landers. Data are from ORP data base and sampling by patent tong occurred in December 2020; data are mean ± standard error. The biomass is dry tissue weight, target biomass is the restoration goal and the percent of samples at the site meeting this criteria is shown, and the reef size for the reef segment is shown. The "All Sites" is the mean and standard error for all 30 sample locations in the Little Choptank River. 13
Table 3. Bromide leakage, oxygen uptake with standard deviation from equation 1.7, leakage estimates from a Matlab fit to oxygen time course, and Matlab oxygen uptake estimate, again without bromide data. 21
Table 4. Calculations for ammonium fluxes. For significance, we show orange shading for significance > 0.10. 28
Table 5. Calculations for NO_x^- fluxes. For significance, we show orange shading for significance > 0.10 and yellow shading for significance between 0.005 and 0.10. 30
Table 6. Calculations for N_2-N fluxes. For significance, we show orange shading for significance > 0.10 and yellow shading for significance between 0.005 and 0.10. 33
Table 7. Calculations for SRP fluxes. For significance, yellow shading for significance between 0.005 and 0.10. 35

List of Figures

Figure 1. The schematic depicts the key features of a bottom lander, with consideration for leakage (inflow = outflow), internal mixing for homogenization and reasonable shear stress, nutrient and gas exchange on the bottom, lighting for light and dark incubations, and a tube for pumping samples to the surface. The right two panels use O_2 to show flux time courses with dilution, with moderate and high rates of O_2 uptake and dilution rates from 0 to 2 h^{-1}. A significant reduction of oxygen concentration ensures ΔN_2 concentrations are sufficient. 7
Figure 2. Photo of lander on boat deck and top view through the acrylic top. 8
Figure 3. Illustration of mop heads attached to an aluminum flange a the bottom of the lander. 9
Figure 4. Three lifting rings and two lifting handles were used to suspend and move the lander. 9
Figure 5. O-ring port for YSI and luer fitting for water sampling. 10
Figure 6. Water pump used for water circulation within the lander. 10
Figure 7. Time course of rhodamine after injection into the chamber. 11
Figure 8. Site locations with characteristics shown in Table 1. 12
Figure 9. Sonar representation of the bottom in the vicinity of our Site 4 (McKeil Point), with a plot of oyster size in 2019 showing most oysters were 60-100 mm in length (2.4-3.9"). Figure is from:

(https://www.chesapeakebay.net/documents/2019_MD_Oyster_Monitoring_Report_FINAL.pdf). Orange represents shallow and green is deep. Note the change in depth within segment L037, decreasing from west to east, toward land. 13
Figure 10. Example oxygen time course showing asymptote (McKeil Pt. Sept 21, 2021). 15
Figure 11. Lander being readied for deployment in the Little Choptank River. Blue peristaltic pump on boat center console is used form sampling with power from orange battery pack (above). 15
Figure 12. Bottom topography at McKeil Point, Little Choptank River. Underwater "drone" (*Chasing Dory*) used for photography, greenish color from algae. 16
Figure 13. Lander on bottom showing mop head sealing the bottom (imperfectly). 16
Figure 14. Top of chamber during deployment. The green stopper and the gray PVC port are used to secure the YSI water quality meter within the chamber. The orange object in the chamber is a submersible pump. 17
Figure 15. Example exponential fit of bromide data over time. 20
Figure 16. Time course of oxygen from McKeil Point on 8/25/2021 (blue points with left axis) and the rate of oxygen uptake estimated on a point to point basis from equation 1.7 21
Figure 17. Plot of oxygen flux rates derived from equation 1.7 using bromide dilution rates, and by fit of the oxygen time course with the curvature of the time course yielding a dilution rate. 22
Figure 18. September 21, 2021 McKeil Point bBromide time course showing total bromide, added bromide and "background" bromide from brackish water. Plot A is for > 2 hours, plot B is for 1 h, and plot C is for 0.5 h. 23
Figure 19. Rate of leakage for 5 lander deployments on multiple dates at McKeil Point in 2021. 23
Figure 20. Leakage data from Susquehanna Point (8/20/2021). Panel A shows the bromide change over time and panel B shows changes in total conductivity and changes in the conductivity from the added bromide. 24
Figure 21. Field oxygen concentrations plotted over time. The numbers correspond to the deployments shown in Table 3. 25
Figure 22. Time courses of ammonium concentration. The plot ID's (1-7) correspond to the data in Table 4. 27
Figure 23. Plot of all ammonium data versus the corresponding oxygen concentrations derived from O_2/Ar measurements. 27
Figure 24. Plot of ammonium data used to estimate NH_4^+ to O_2 ratios. The lines are from linear regression and the slope and intercept are shown in Table 4. 28
Figure 25. Time courses of NO_x- (nitrate + nitrite) concentration. The plot ID's (1-7) correspond to the data in Table 5. 29
Figure 26. Plot of all NO_x^- data versus the corresponding oxygen concentrations derived from O_2/Ar measurements. 30
Figure 27. Plot of NO_x^- data used to estimate NO_x^- to O_2 ratios. The lines are from linear regression and the slope and intercept are shown in Table 5. 31
Figure 28. Time courses of N_2 concentration. The plot ID's (1-7) correspond to the data in Table 6. 32
Figure 29. Plot of all N_2 data versus the corresponding oxygen concentrations derived for O_2/Ar measurements. 32

Figure 30. Plot of N_2 data used to estimate N_2 to O_2 ratios. The lines are from linear regression and the slope and intercept are shown in Table 6. 33
Figure 31. Time courses of SRP concentration. The plot ID's (1-7) correspond to the data in Table 7. 34
Figure 32. Plot of all SRP data versus the corresponding oxygen concentrations derived for O_2/Ar measurements. 35
Figure 33. Plot of SRP data used to estimate SRP to O_2 ratios. The lines are from linear regression and the slope and intercept are shown in Table 7. 36
Figure 34. Stacked bar plot of all N fluxes. Note that some of the rates were not significant. 37
Figure 35. Box plots of oxygen fluxes and N_2-N fluxes from Harris Creek, a mid-Choptank site (Kellogg et al. 2013) and this study. The Harris Creek data is from summer and early fall, as is the Kellogg data. 37
Figure 36. Plot of the sum of nitrogen flux species (NO_x^-, NH_4^+, N_2-N McKeil Point and other Little Choptank sites, summer and fall 2015 in Harris Creek, summer data from the upper Choptank (Kellogg et al. 2013), all compared to a plot of the expected ratio of total N remineralization to O_2 flux (0.151), assuming that O_2 reflects total carbon remineralization. 38
Figure 37. Biomass and denitrification relationship in oyster denitrification BMP (in progress). The red arrow shows the biomass at the Little Choptank sites, plotted on the summer subtidal plot. Data and figure were developed by Lisa Kellogg (VIMS). 39
Figure 38. Time course of oxygen over ~ 2 hours. The data shown for showed a decrease of 23 μmol L^{-1} over the first half hour, 11 over the next half hour and only 7 over the next hour. 41
Figure 39. Plot of the standard error for estimated oxygen fluxes as a function of the leakage rate. 41

Introduction

Background

The ecosystem services provided by oysters have been the subject of numerous investigations over the last 3 decades. In nutrient-impaired coastal ecosystems, the need for additional Best Management Practices (BMP) to facilitate meeting Total Maximum Daily Load targets has directly led to the idea that nitrogen removal by oysters may help in nutrient mitigation ((Kellogg et al. 2014, Rose et al. 2014). In the Chesapeake, the only approved BMP for oysters nutrient removal is from the removal of N and P in the tissue of cultured oysters (Cornwell et al. 2016), with the BMP expert panel considering denitrification as one of 3 other potential BMP's. Default estimates, indexed to oyster biomass, are under consideration, largely based on the large-scale restoration at Harris Creek (https://chesapeakebaymagazine.com/study-harris-creek-oyster-recovery-delivers-stunning-results/).

Denitrification can generally be considered the conversion of organic and dissolved inorganic forms (solutes) of nitrogen to N_2 (di-nitrogen gas) and N_2O (nitrous oxide, generally a minor pathway). For the purposes of this report, we consider denitrification to be the rate of production of N_2.

The measurement of benthic denitrification has evolved since the 1970's, with modern approaches generally using ^{15}N tracers or the N_2:Ar gas ratio change over time during sediment incubations (Nielsen 1992, Seitzinger et al. 1993, Kana et al. 1998). Early N_2:Ar-based studies used simulated biodeposit additions (Newell et al. 2002) and reef-adjacent sediment core incubations (Piehler and Smyth 2011) to examine oyster-related denitrification rates. These approaches without inclusion of oysters likely underestimate denitrification because a substantial proportion of denitrification appears to be associated with oysters and their shell ecosystem (Caffrey et al. 2016, Jackson et al. 2018). Our *ex-situ* incubation approach (Kellogg et al. 2013), using trays that include both sediment and oysters embedded in the substrate, was the first to use the whole community; subsequently *in situ* chamber observations using long-term embedded bases have been used in New England (Humphries et al. 2016).

Need for a New Approach

Our *ex situ* approach and the *in situ* approach both are manpower intensive, with our measurements at Harris Creek requiring a team of divers and support personnel to embed and recover the trays, plus a team to carry out dark and light incubations. A conservative estimate of effort, not including the chemical and data analyses, is ~ 2 person days per rate measurement. This approach has yielded considerable understanding of rates on a measured biomass basis, but likely makes the measurement too expensive for routine management applications. **Our goal is to develop an *in situ* chamber approach to decrease the field and incubation personnel effort 3-4 fold and make the measurement of denitrification affordable for management purposes. We propose to develop and test a viable measurement system that is lowered to the bottom, does not require divers, and in which two individuals can operate two chambers simultaneously.**

Tethered and un-tethered landers have been used in coastal and deep-sea environments to make measurements of sediment nutrient and gas exchange (Kemp and Boynton 1984, Berelson et al. 1998). A fundamental requirement of landers is that the bottom edge be sealed so that over a time course of sample collection there is no exchange with the outside environment. However, that requirement is difficult to attain in an oyster reef because the surface is not uniform. Given the high likelihood that the chamber will not completely seal, time course data within the chamber necessarily requires an understanding of the rate of leakage. The general circumstance is depicted in Figure 1 in which the number we desire is the biogeochemical bottom exchange rate and the rates of inflow and outflow are the leakage rate. Modeled sets of oxygen time courses for two oxygen uptake rates are presented for different leakage rates in chamber volumes per hour, based on the solution of a differential equation describing a well-mixed reactor. Oxygen decreases over time are muted by higher rates of dilution, but with these realistic rates of oxygen uptake we have sufficient sensitivity for accurate measurement at dilution rates up to twice the volume of the chamber per hour.

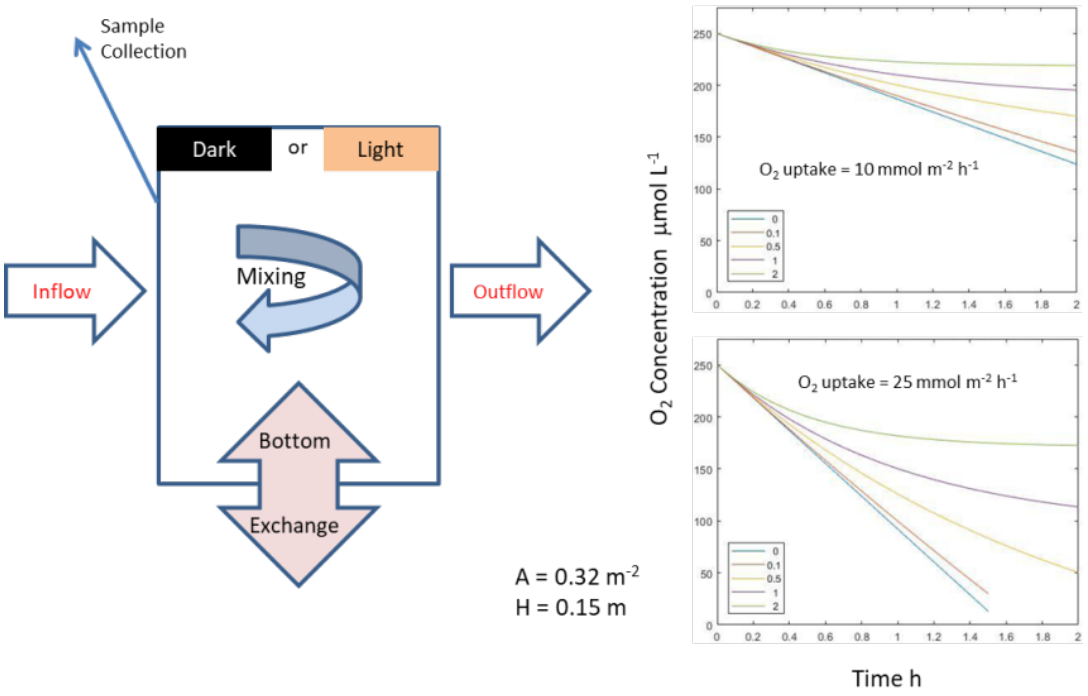

Figure 1. The schematic depicts the key features of a bottom lander, with consideration for leakage (inflow = outflow), internal mixing for homogenization and reasonable shear stress, nutrient and gas exchange on the bottom, lighting for light and dark incubations, and a tube for pumping samples to the surface. The right two panels use O_2 to show flux time courses with dilution, with moderate and high rates of O_2 uptake and dilution rates from 0 to 2 h^{-1}. A significant reduction of oxygen concentration ensures ΔN_2 concentrations are sufficient.

Approach Overview

Determination of the bottom exchange rates thus requires knowledge of the leakage rate and external oxygen concentration. The leakage rate may be estimated by a time course of conservative tracer concentrations, or by imposition of flow via a pump in which the imposed flow controls the leakage rate,

or both. External oxygen concentrations and nutrient concentrations should be measured. We have used bromide (Br-), a normal sea water constituent that we add in excess of normal concentrations, as a tracer in other sediment flux applications (Owens and Cornwell 2020) and use it in this approach to estimate the leakage rate. The initial laboratory testing regime included estimating the mixing regime in the chamber, using "skirt" materials to seal the bottom as tightly as possible, and tracer application as a single "bolus". Field performance verification was carried out on the restored oyster reef in the Little Choptank River. Measurements included continuous monitoring of dissolved oxygen and discrete time course sampling of N_2 (denitrification) determined from N_2:Ar ratios, oxygen, ammonium, nitrate plus nitrite, and soluble reactive phosphorus..

Methods

Chamber Construction

Relative to the construction of the *ex-situ* chambers previously used in the Choptank River (Kellogg et al. 2013, Jackson et al. 2018, Cornwell et al. 2019, Bruce et al. 2021), the construction of the *in-situ* benthic lander was relatively simple. A 24" diameter (60cm) od pvc pipe, with 0.75" wall thickness (1.9 cm) was used, with a height of 18" (45.72cm). the areal coverage of the lander is 0.283 m2 and the volume is 129.2 L or 0.129 m^3. The acrylic top was 0.5" thick (1.3 cm). The overall structure is illustrated in Figure 2.

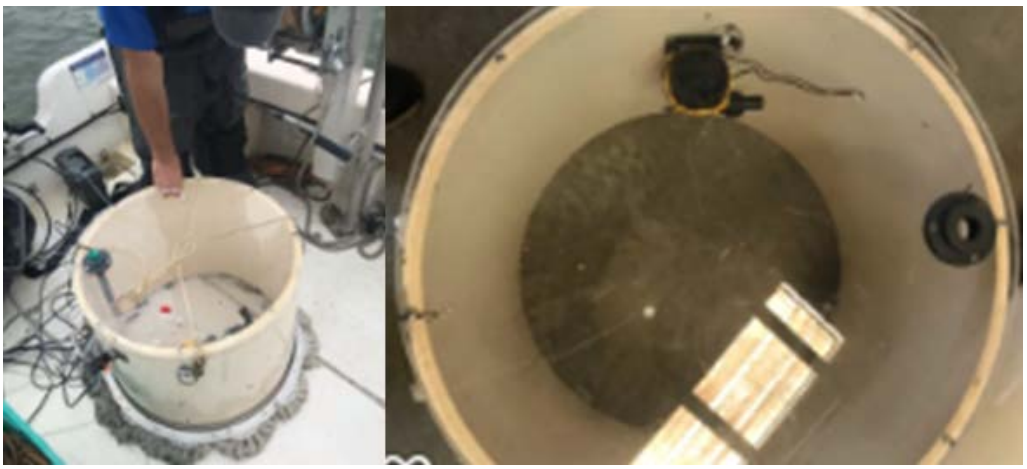

Figure 2. Photo of lander on boat deck and top view through the acrylic top.

The bottom of the lander had an aluminum flange attached to support the lander on the substrate and to attach the mop heads used to help seal the lander bottom.

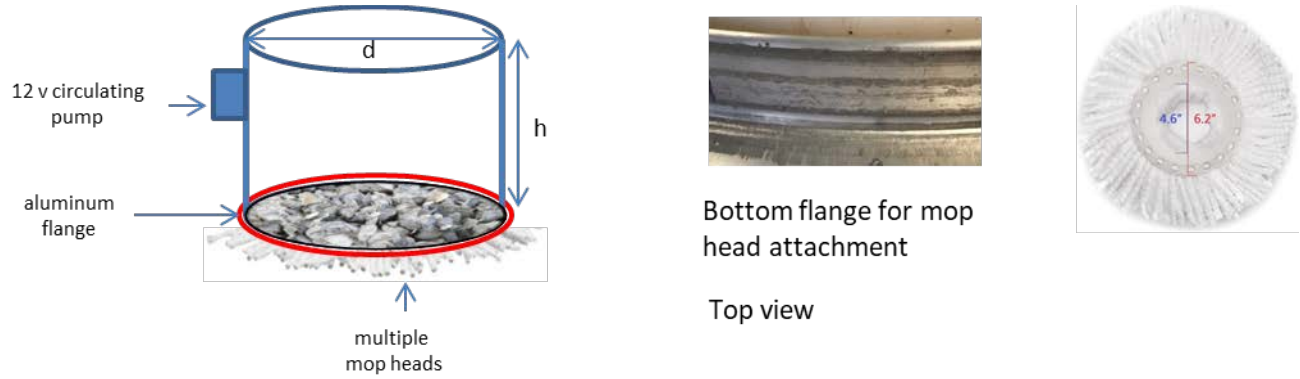

Figure 3. Illustration of mop heads attached to an aluminum flange to the bottom of the lander.

Lifting handles were used to load the lander on the boat and to position the lander for deployment (Figure 4. Lifting rings were attached to enable securing the lander to the winch via rope.

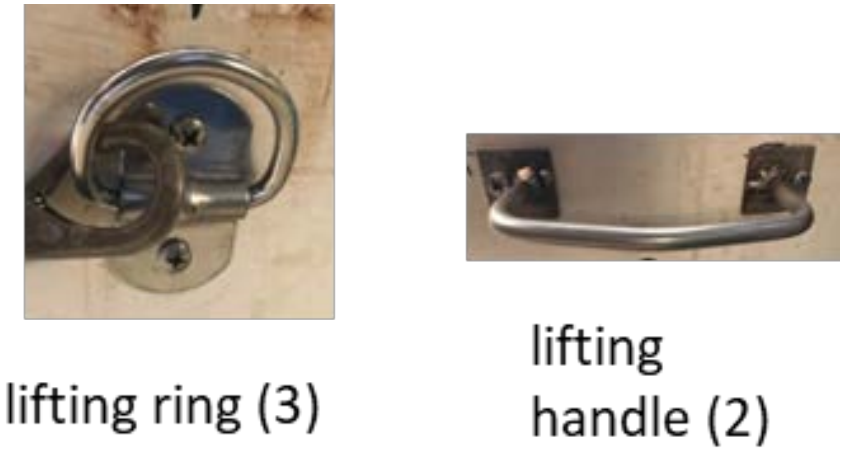

Figure 4. Three lifting rings and two lifting handles were used to suspend and move the lander.

The YSI water quality sonde was placed within the tank using an o-ring port (Figure 4). A stopper with a hole drilled in the center and slit to the edge, can also be used. Luer fittings were used to attach tubing to the lande to 1) add bromide from above and 2) sample the lander water column for dissolved nutrients and gases.

o-ring port
for YSI

Luer fitting

Figure 5. O-ring port for YSI and luer fitting for water sampling.

A 300 gph 12v pump (Figure 6) was attached to the inside of the tank and used for circulation of the water. This contrasts with the propeller design used by Kellogg et al. (2013) for ex-situ incubations. Although propeller-driven circulation was considered, it was not tested because the pump system was robust and similar systems have been used in previous coastal benthic studies (Boynton et al. 1981, Fisher et al. 1982).

Figure 6. Water pump used for water circulation within the lander.

The materials list for the lander system is presented in Appendix I. The basic lander system cost <$1,000 for materials and a little more than $1,000 for labor by the UMCES machinist. The sampling system, including pumps and batteries, added <$400. One of the bigger expenses was a YSI Prosolo sonde with a 20 m cable; two sondes are preferable to measure oxygen both inside and outside the chamber.

Mixing Experiments

We carried out two experiments with rhodamine dye to determine if mixing was sufficient. (Figure 6). The experiment took place in large tank full of filtered sea water (i.e. particle free) and it mixing appears complete in < 2 minutes. Sampling took place in the sampling port in the chamber, the location where all samples are collected for nutrients and gases.

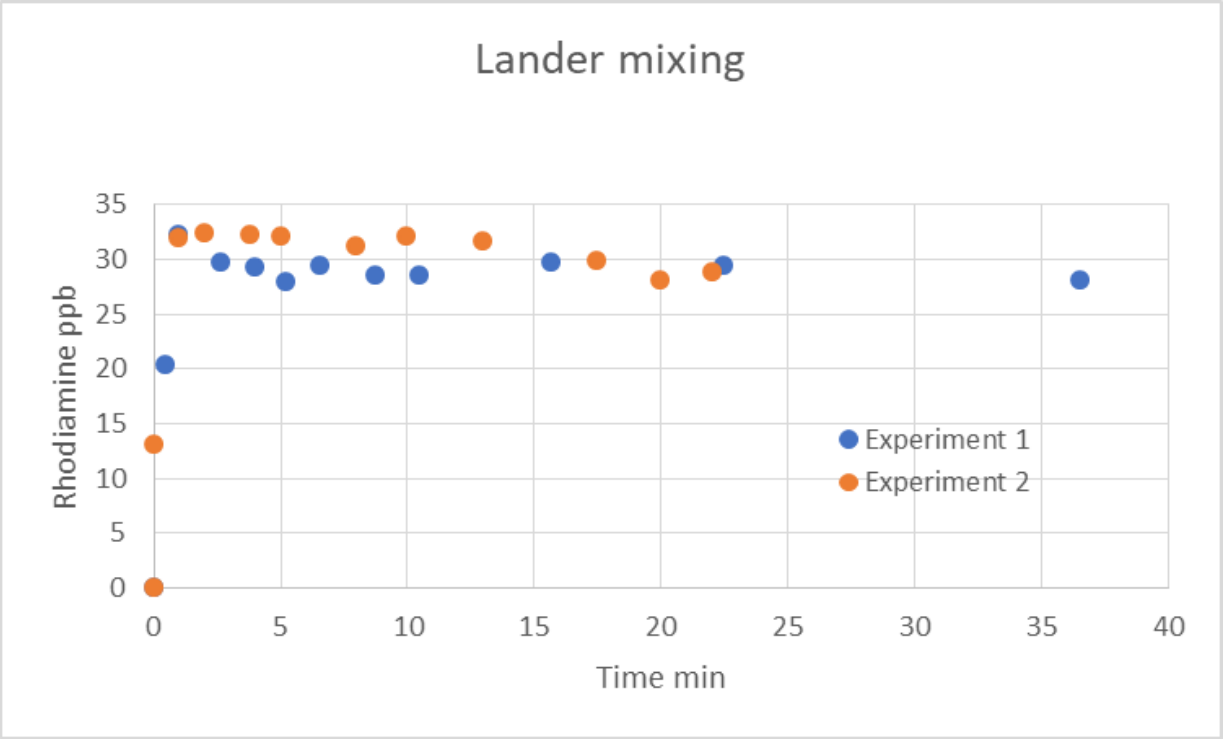

Figure 7. Time course of rhodamine after injection into the chamber.

Field Deployments

Sites and Characteristics

The Little Choptank oyster sanctuary consists of series of reef segments (Figure 1) that are found throughout the central area of the subestuary. The area of restored bottom, with spat on shell, consists of 358 acres, with all completed by the end of 2020 (https://oysterrecovery.org/little-choptank/). Most Little Choptank reefs were 3 years old in 2019 at the time of initial characterization; a sonar characterization of one of the sites (our site 4) is shown in Figure 2.

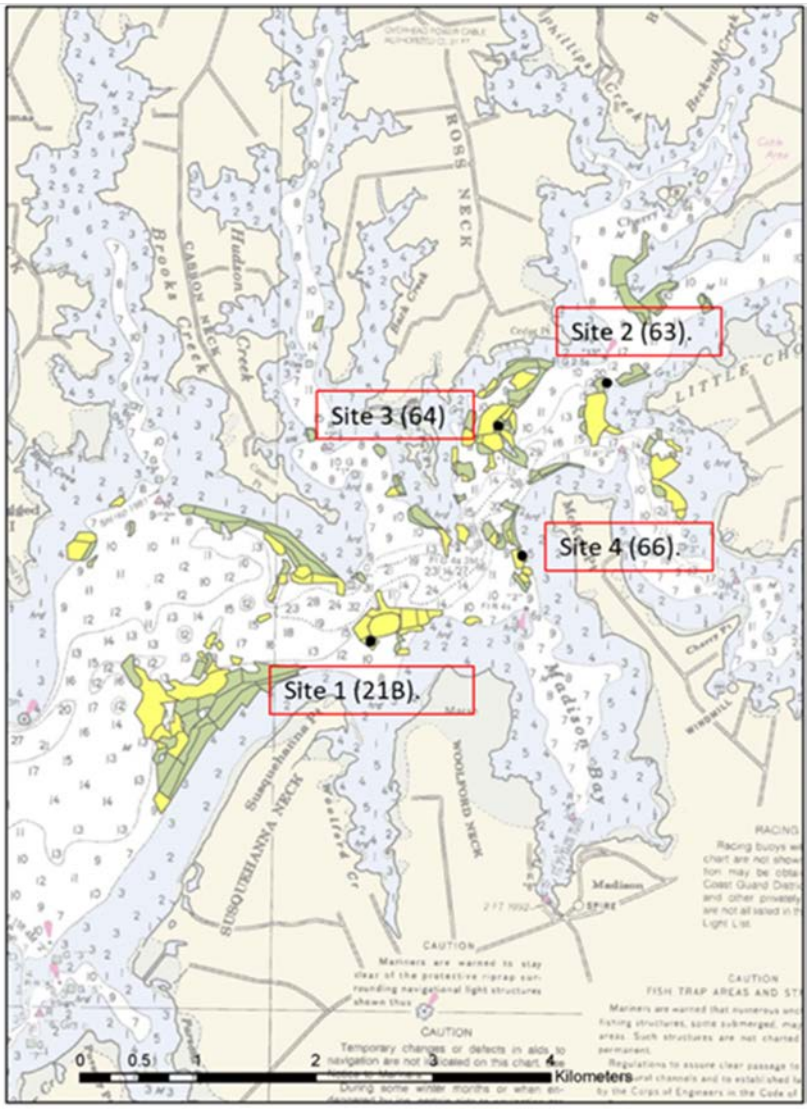

Figure 8. Site locations with characteristics shown in Table 1.

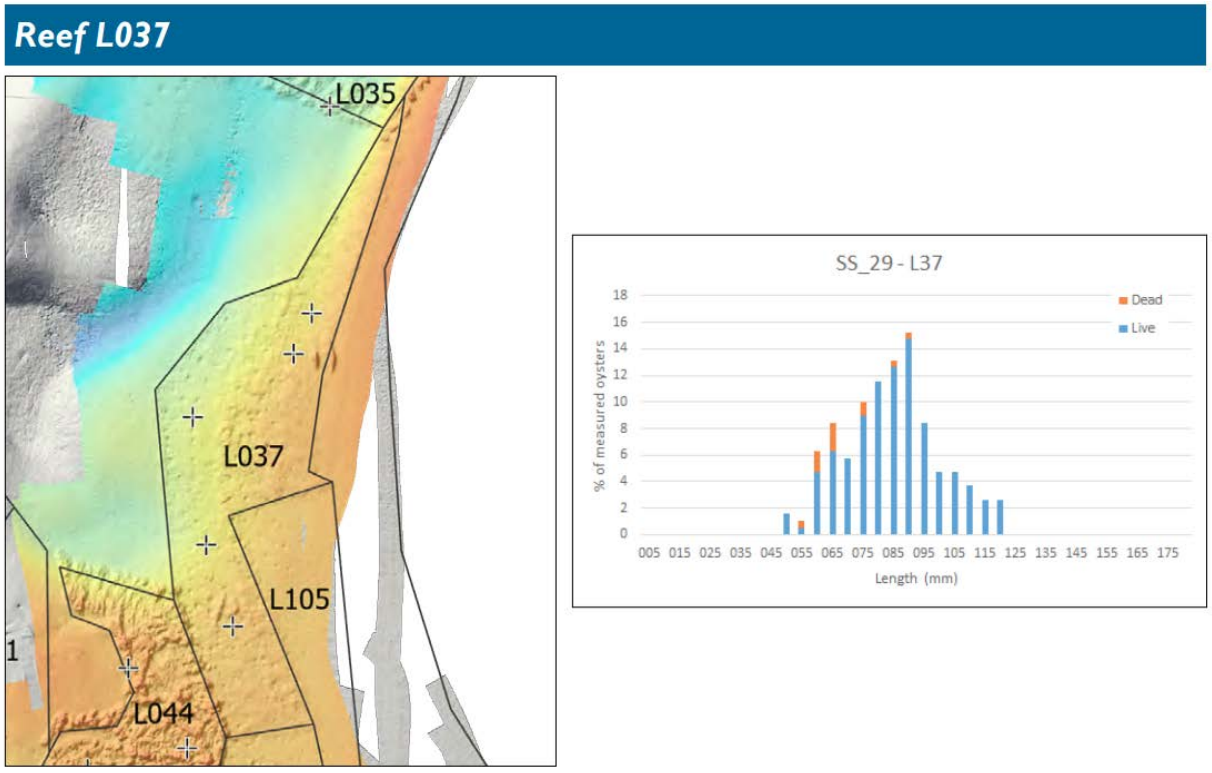

Figure 9. Sonar representation of the bottom in the vicinity of our Site 4 (McKeil Point), with a plot of oyster size in 2019 showing most oysters were 60-100 mm in length (2.4-3.9"). Figure is from: (https://www.chesapeakebay.net/documents/2019_MD_Oyster_Monitoring_Report_FINAL.pdf). Orange represents shallow and green is deep. Note the change in depth within segment L037, decreasing from west to east, toward land.

The choice of the four sites used in this study was described in the previous CBT report, and all sample events are listed here in Table 1 and their oyster restoration success presented in Table 2:

Table 1. Lander deployments. Note that replicates were done on 8/25 and 9/17, with two sites within 10 m of each other.

Date	Site (map #)	Site Name	Br^- Leakage	O_2 uptake
			h^{-1}	mmol m^{-2} h^{-1}
8/20/2021	4	Mckeil Pt	1.272	37.57
8/25/2021	4	Mckeil Pt a	0.505	26.58
8/25/2021	4	Mckeil Pt b	0.825	43.02
9/17/2021	1	Susquehanna Pt	1.956	10.12
9/17/2021	1	Susquehana Pt b	2.568	26.76
9/21/2021	2	Town Pt	0.586	9.13
9/21/2021	4	Mckeil Pt	0.925	23.43

Table 2. Site characteristics from 4 sites used for testing landers. Data are from ORP data base and sampling by patent tong occurred in December 2020; data are mean ± standard error. The biomass is dry tissue weight, target biomass is the restoration goal and the percent of samples at the site meeting this criteria is shown, and the reef size for the reef segment is shown. The "All Sites" is the mean and standard error for all 30 sample locations in the Little Choptank River.

Site	Initial Planting Year	Minimum Target Biomass?	Biomass 2020	Count 2020	% Market Size	Reef Size	Dates Occupied	Deployments
			g dw m^{-2}	# m^{-2}	%	Acres		
1 (21B)	2016	✓	123±13	246±30	29	2.6		
2 (63)	2016	✓	122±28	311±66	20	0.2		
3 (64)	2016	✓	121±22	237±30	24	2.0		
4 (66)	2016	✓	112±15	277±24	17	0.9		
All Sites	2016	✓	72±5	145±13	33±2	3.6±0.7		

Deployment Protocol

The successful field deployment requires considerable coordination of a number of different systems:

1. Boat/anchoring: Even with the relatively shallow water depths (< 4 m) associated with Chesapeake Bay oyster restoration, anchoring is one of the most challenging aspects of making benthic chamber measurements. We used a 21' Wetsig boat ($150 per day + fuel) that was equipped with a davit suited to heavy lifting (< 100 kg). Depending on the wind or tide, the boat was oriented into the overall flow, the front anchor was dropped ~20 m from the desired location, and the boat was released back to where that anchor holds. The boat was backed left and right, with anchors deployed laterally. This 3 point anchoring is essential because we could move more that 2-3 m before pulling the deployment cables and tubing taut, potentially tipping the lander. Furthermore, with the data usage being tied to the independently-measured oyster biomass, staying on site where biomass is known is essential.
2. Lander set up: prior to deployment, it was critical to ensure the mixing system was functional, the YSI measurement system inside the chamber was working, and that all sample tubing, electrical feeds, and instrument cables were not tangled.
3. When the lander was hung on the cable above the water, we ensured all connections were safe. Upon lowering it into the water, we manually tilted the chamber to allow water to flood into the chamber, and ensured we do not trap air in the chamber. The clear top allowed us to observe air bubbles and correct that issue.
4. The chamber was slowly lowered, with 1-2 minutes until it reached the bed. The YSI continually monitored the oxygen level and concentrations decreases were generally observed from the outset. The YSI oxygen, salinity and temperature readings were recorded at 1 minute intervals.
5. Bromide was added as a tracer of leakage and is added via a separate tubing line. To ensure air bubbles were not added, water is drawn by a 60 mL syringe into the tubing to a valve which is closed. Bromide (60 mL) is pushed into the tubing after opening the valve; an additional flush of 60 mL of surface water was pushed into the chamber to ensure no bromide remained in the tubing. After 1-2 minutes, our sampling for nutrients and N_2 was initiated.
6. A peristaltic sampling pump was used to sample the chamber, with an initial high flow to clear the tubing and keep residence time in the tubing to a minimum. In between sampling steps, the

pump was slowed down. Initial samples were overflowed into 7 mL glass vials for gas analysis, with 10 µl of half-saturated $HgCl_2$ added to stop any microbial transformations. After gas preservation, a 30 mL plastic syringe, with the bottom blocked by a 0.4 mm syringe filter, was filled and the plunger placed in the syringe barrel. Individual vials were filled with filtered water, each with 5 mL (1 vial each for bromide, nitrate+nitrite, ammonium, and soluble reactive phosphorus). Gas samples were stored under water to ensure the stopper did not dry out and that temperatures did not increase greatly. The dissolved nutrient samples were kept on ice until they were frozen upon return to the laboratory.

7. The length of deployment was determined by the oxygen concentration changes. Without leakage, changes would be linear over time and at summer rates of metabolism, would require < 1 hour of deployment. With leakage, the oxygen decrease is a curve that eventually becomes asymptotic (Figure 2); at that point, no further information can be gleaned from the incubation.
8. The chamber was retrieved and brought to the surface. For a duplicate deployment, the anchor line can be picked up, the boat moved a short distance, the anchor re-deployed and the chamber set back on the bottom.

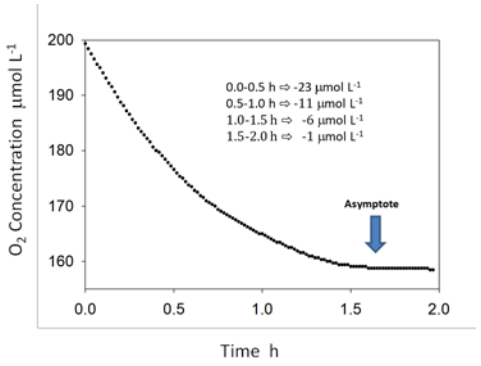

.

Figure 10. Example oxygen time course showing asymptote (McKeil Pt. Sept 21, 2021).

Figure 11. Lander being readied for deployment in the Little Choptank River. Blue peristaltic pump on boat center console is used form sampling with power from orange battery pack (above).

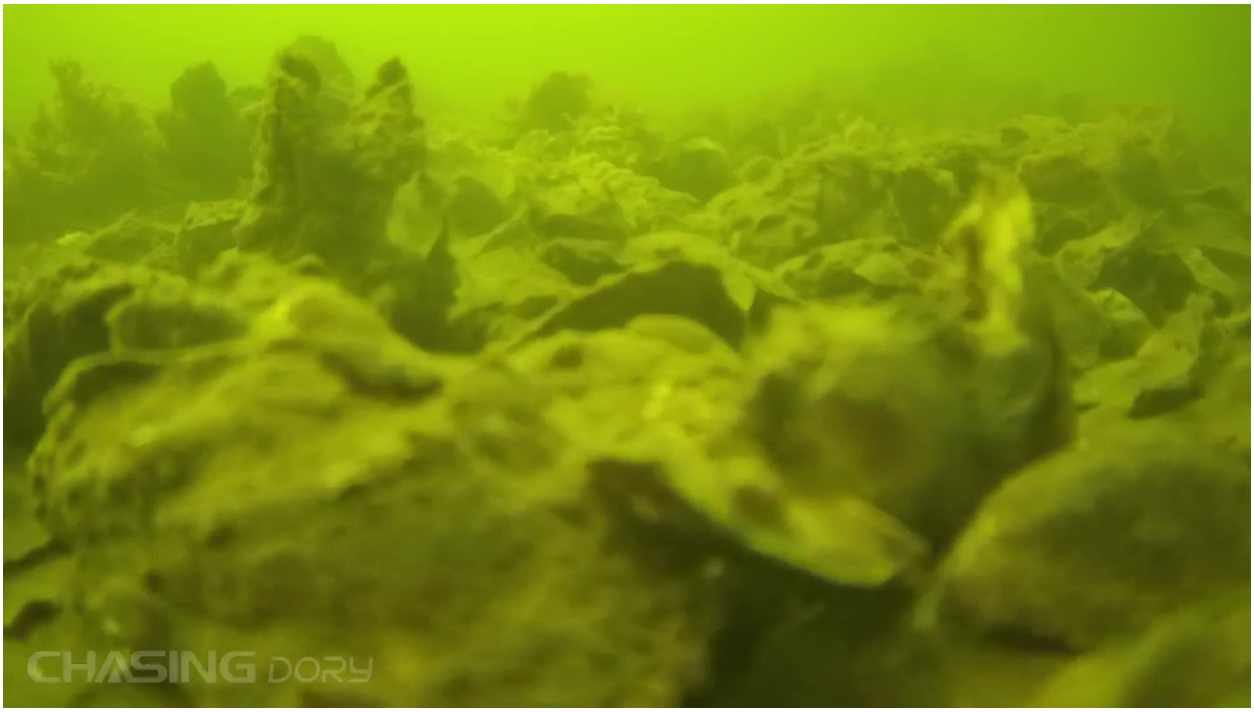

Figure 12. Bottom topography at McKeil Point, Little Choptank River. Underwater "drone" (*Chasing Dory*) used for photography, greenish color from algae.

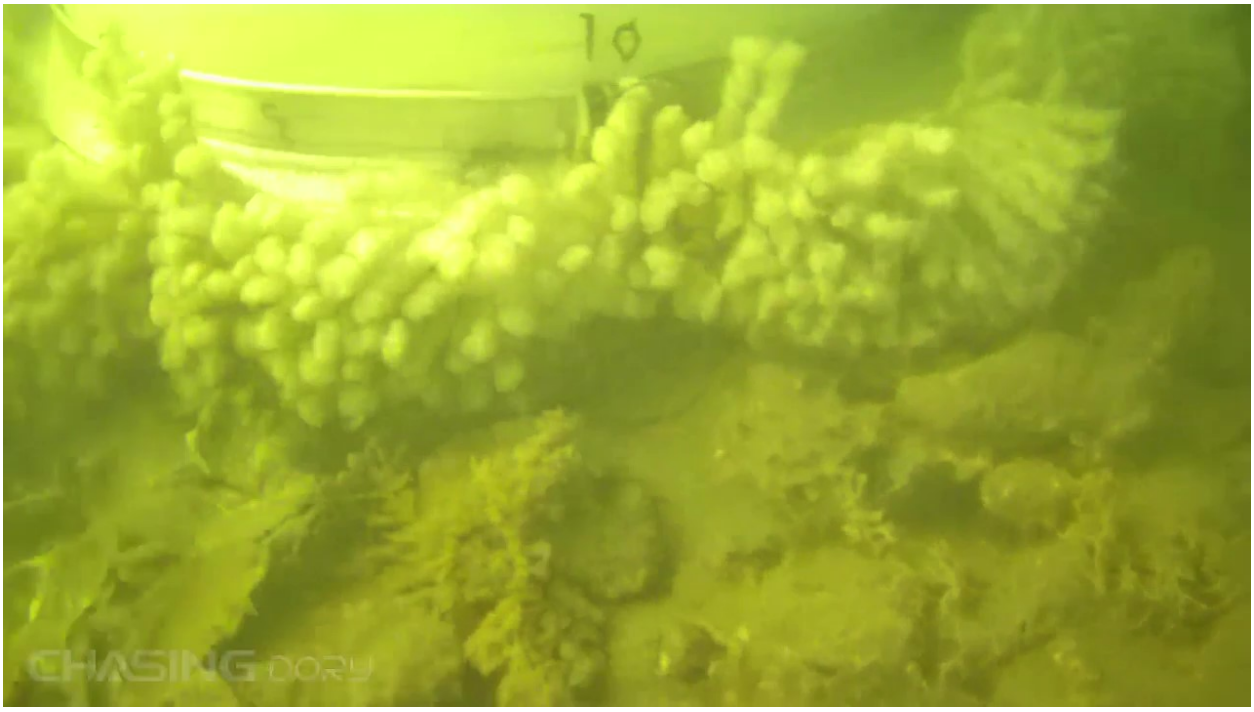

Figure 13. Lander on bottom showing mop head sealing the bottom (imperfectly).

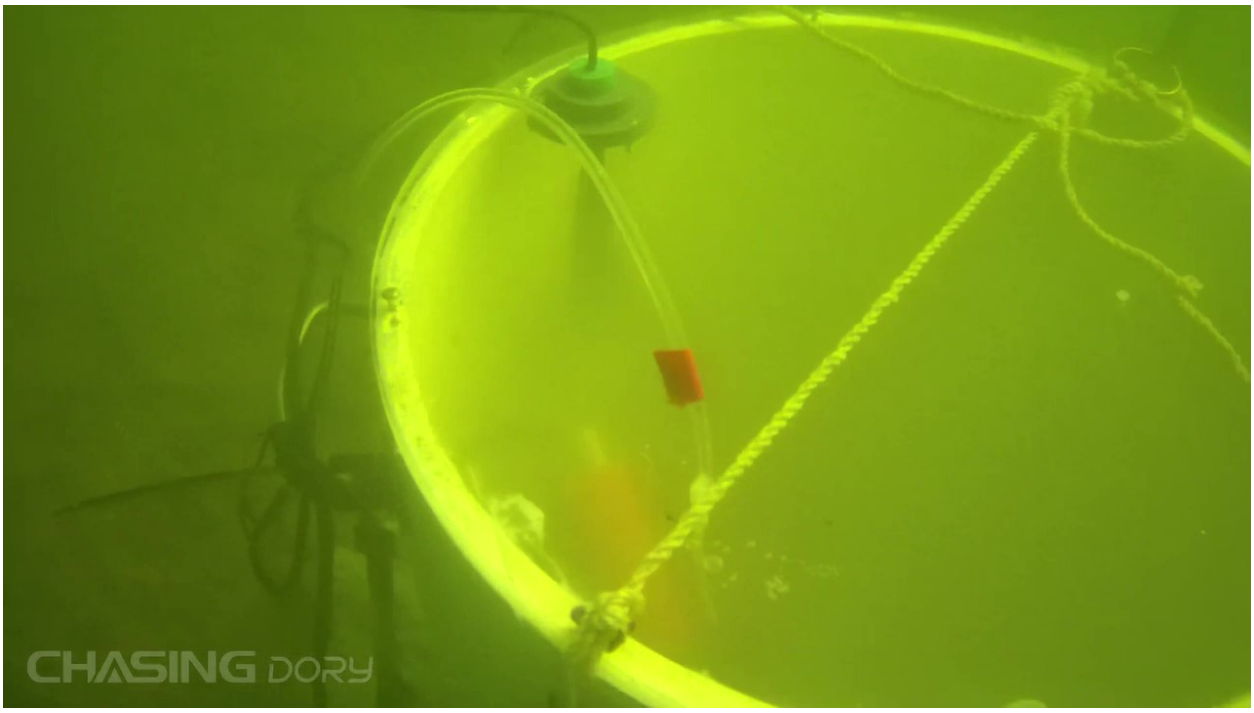

Figure 14. Top of chamber during deployment. The green stopper and the gray PVC port are used to secure the YSI water quality meter within the chamber. The orange object in the chamber is a submersible pump.

Sample Collection and Analysis

Field samples were collected using a peristaltic pump connected to the chamber. The sampling time was recorded in a notebook and tubes for gas analysis filled and preserved (see below). For dissolved nutrient collection, water was pumped into a 20 mL plastic syringe with the plunger removed and an attached 25 mm diameter, 0.4mm pore size syringe filter attached. After filling the syringe, the plunger was inserted and the water filtered into 7 mL plastic vials. A total of 4 vials were filled with 5 mL of samples for analysis of ammonium, nitrate plus nitrate, soluble reactive phosphorus, and bromide. Samples were kept cold in a cooler on the boat until frozen at the Horn Point Laboratory.

Todd Kana's laboratory at HPL developed a high precision rapid method for dissolved gases (N_2, O_2, and Ar) using membrane inlet mass spectrometry (Kana et al. 1994) and the technology is now used in >> 20 laboratories worldwide for denitrification and microbial metabolism research. This method has been routinely used in Cornwell's laboratory over the last two decades for measuring denitrification in sediments and oxygen-cycling in photosynthetic and non-photosynthetic benthic systems (Cornwell et al. 1999, Kellogg et al. 2013, Cornwell et al. 2016, Owens and Cornwell 2016, Owens and Cornwell 2020, Owens et al. 2021).

High precision measurement of dissolved gases involved the following: Samples were collected in 7 ml stoppered test tubes. These water samples were preserved using $HgCl_2$ to preserve samples for analysis

within < 3 weeks. The sample was analyzed by pumping the water through a membrane tube situated inside the mass spectrometer vacuum. In practice, it required ca. 1-2 minutes for a measurement to be completed. Generally, individual gas concentrations were measured with a precision of 0.1-0.2% c.v. and gas ratios (e.g. N_2/Ar) can be measured with a precision of 0.02-0.03% c.v. Week to week repeatability for O_2 concentration has been determined to be better than 0.2% c.v.

Argon-normalized gas ratios were converted to gas concentrations by multiplying the gas ratio by the Ar concentration assuming Ar is in air equilibrium. Mass spectrometer discrimination for the gas of interest relative to Ar was determined from measurements of air equilibrated standards. The standards were prepared using deionized water held to a temperature tolerance of ±0.02^{o}C with 100% relative humidity in the head space. Standards were stirred, not bubbled. This technique has proven highly accurate and reproducible. We replicated analyses on the initial sampling (i.e. time zero) from each core.

Dissolved nutrient samples were analyzed colorimetrically for soluble reactive phosphorus (Parsons et al. 1984), ammonium (Parsons et al. 1984) and nitrate plus nitrite (Garcia-Robledo et al. 2014), with the latter analysis a using vanadium reductant to reduce nitrate to nitrite prior to analysis. We attempted to use Rhodamine B as a tracer for water exchange (leakage) during the initial phase of the work; adsorption to particulates was much higher than anticipated. Rhodamine analysis used a Rhodamine channel on a Turner Designs fluorometer. Bromide was an effective tracer of leakage and with additions of as NaBr to a final chamber concentration of 150-200 mg L^{-1} Br^{-} and analysis via ion chromatography (Owens and Cornwell 2020).

The YSI sonde used in the chamber was a Prosolo unit (#626650, https://www.ysi.com/prosolo-odo) with a probe assembly (#627150-20) that included an optical oxygen sensor, a conductivity sensor for salinity, and temperature sensor on a 20 m cable. The data system for this unit had an internal clock, data storage capability, and was set to record data at 1 minute intervals. Data was downloaded to a memory stick using proprietary KorDSS software.

Calculations

Traditionally, landers require the bottom edge be sealed so that over the time course of sample collection there is no water exchange with the outside environment. However, that requirement is difficult to attain in an oyster reef because the surface is not uniform. Given the high likelihood that the chamber will not completely seal, using time course nutrient and gas data within the chamber for rate determination requires an understanding of the rate of leakage (dilution). This section presents development of a simple model that extends traditional lander data analysis assuming a sealed bottom to account for leakage.

The general circumstance was depicted in Figure 1 in which the number we desire is the biogeochemical bottom exchange rate, the equal rates of inflow and outflow represent the leakage rate, the chamber is assumed to be well mixed, and the sample collection rate is negligibly small. For the sake of

development, we assume that the quantity of interest is dissolved oxygen concentration, but it could be any dissolved quantity subject to uptake or release across the bottom. With no leakage, and assuming sediment oxygen demand remains constant over the duration of the experiment, oxygen mass decreases at a constant rate over time as

$$\frac{d(Vc(t))}{dt} = -AR \tag{1.1}$$

Where V is the volume of the chamber in m^3, c(t) is the oxygen concentration in umol L^{-1} (=mmol m^{-3}), t is time in hr, R is the desired sediment oxygen demand in mmol $m^{-2}h^{-1}$, and A is the sediment surface area in m^2. Dividing both sides of the equation by V yields

$$\frac{dc(t)}{dt} = -\frac{R}{h} \tag{1.2}$$

Where h is the height of the chamber in m. The solution to eq 1.2 is a linear rate of oxygen decrease in the chamber:

$$c(t) = c(0) - \frac{R}{h}t \tag{1.3}$$

Then simple linear regression of c versus t and division by h yields the desired rate R.

If, however, the seal around the bottom of the lander is not perfect and leakage dilutes internal water with external water, then both the rate of leakage and the difference between internal and external concentrations must be accounted for to derive an estimate of R. The governing equation becomes

$$\frac{d(c_{in}(t))}{dt} = \frac{F}{V}c_{out}(t) - \frac{F}{V}c_{in}(t) - \frac{R}{h} \tag{1.4}$$

Where F is the leakage rate in m^3h^{-1}, c_{in} is the concentration inside the chamber and c_{out} is the concentration outside the chamber.

Assuming that c_{out} remains constant over the duration of the experiment and that $c_{in}(0) = c_{out}$, the solution to eq 1.4 is

$$c_{in}(t) = c_{in}(0) - \frac{R}{h}\frac{V}{F}\left(1 - e^{-\frac{F}{V}t}\right) \tag{1.5}$$

Which reduces identically to eq 1.3 when Ft/V becomes vanishingly small (i.e., if leakage is negligible and/or at very short times). Example solutions of eq 1.5 are presented in Figure 15 using our chamber dimensions for two oxygen uptake rates and a range of leakage rates. Oxygen decreases over time are muted by higher rates of leakage, but knowledge of the leakage rate still permits solving for the desired uptake rate in most situations.

The leakage rate may be estimated from a separate time course of an injected conservative tracer concentration, or by nonlinear curve fitting to the observed oxygen time record, or both. We tried both approaches. We used bromide (Br-), a conservative sea water constituent added as a small excess spike inside the chamber at t=0 and sampled at approximately 10 min intervals as a tracer (e.g. Owens and Cornwell 2020) to estimate the leakage rate. We also fit the full version of equation 1.5 to observed oxygen time courses using the Matlab© nonlinear curve fitting toolbox.

An example of leakage rate estimation using Br- is shown in Figure 15, where excess Br- (ΔBr-) in mg L^{-1} is plotted over time for the second chamber experiment at McKeil Pt on 8/25/2021. The data are fit to a dilution equation of the form

$$\Delta\text{Br-} = \Delta\text{Br-}(0)e^{-\frac{F}{V}t} \tag{1.6}$$

yielding an estimate of F/V = 0.825 h^{-1} with r^2=0.99. The most straightforward way to apply this leakage rate to the oxygen data is to solve eq 1.5 for R, yielding

$$R = \frac{h(c_{in}(0) - c_{in}(t))}{\frac{V}{F}\left(1 - e^{-\frac{F}{V}t}\right)} \tag{1.7}$$

Eq 1.7, when applied to the oxygen time series shown in Fig 16 collected simultaneously with the Br- data of Fig 16, yields estimates of R also shown in Figure 16. The average R estimate is 43.0 mmol $m^{-2}h^{-1}$ with a standard deviation of 1.5 mmol $m^{-2}h^{-1}$.

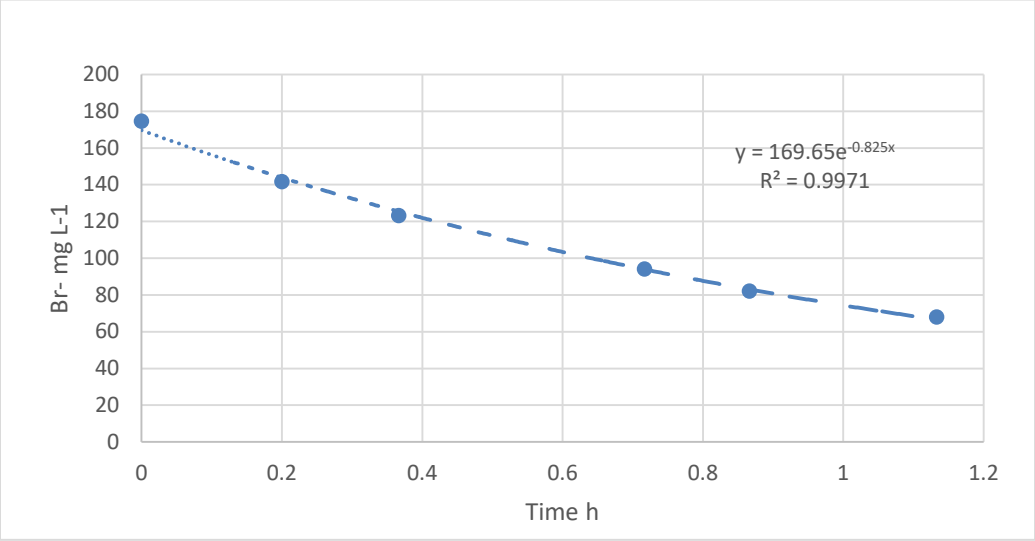

Figure 15. Example exponential fit of bromide data over time.

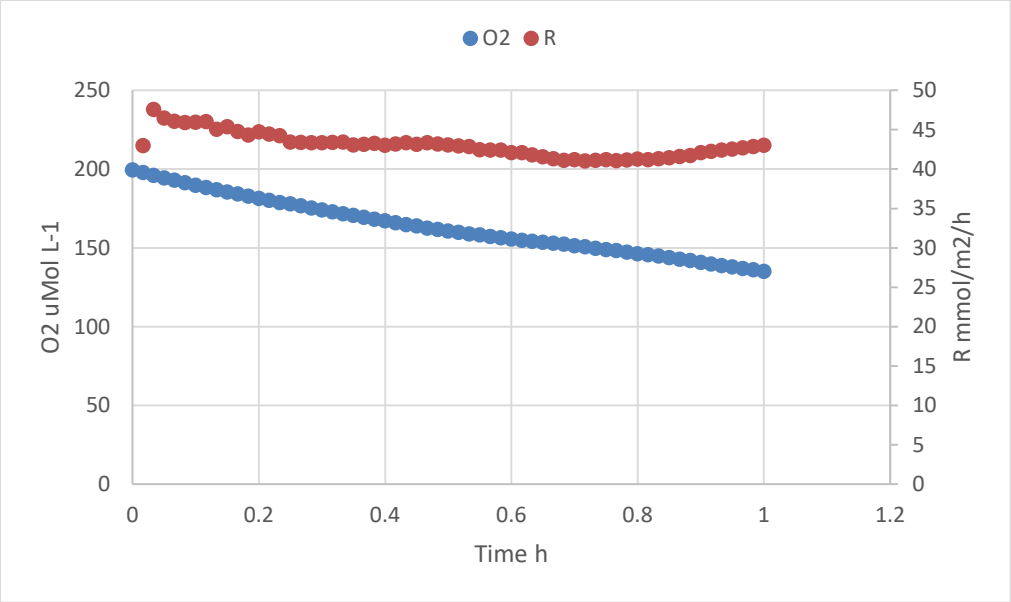

Figure 16. Time course of oxygen from McKeil Point on 8/25/2021 (blue points with left axis) and the rate of oxygen uptake estimated on a point to point basis from equation 1.7.

A direct fit of eq 1.5 to the oxygen time series of Fig 3 using the Matlab© nonlinear curve fitting toolbox and solving for best fit values of R and F/V gives F/V = 0.745 hr^{-1} and R = 40.14 mmol $m^{-2}h^{-1}$ with r^2 = 0.998. These values are similar to those derived from eq 1.7, but not identical.

Table 1 compares the two estimation methods. Remarkably, though the estimates of leakage rate differ considerably between the two methods in some cases, the estimates of O_2 uptake rate are much more similar (Fig 4). Leakage rate directly estimated from a conservative dissolved tracer is unambiguous, and eq 1.7 is the most straightforward to apply for estimates of uptake rate, so for present purposes we adopt these approaches. Potential sources of uncertainty and possible refinements are discussed below.

Table 3. Bromide leakage, oxygen uptake with standard deviation from equation 1.7, leakage estimates from a Matlab fit to oxygen time course, and Matlab oxygen uptake estimate, again without bromide data.

	Date	Reef	Br- leakage rate (h^{-1}) Eq 1.6	O_2 uptake rate mmol m^{-2} h^{-1} Eq 1.7	Std Dev of O_2 uptake estimate	Matlab NL fit leakage rate (h^{-1})	Matlab NL fit O_2 flux mmol m^{-2} h^{-1}
1	8/20/2021	McKeil Pt	1.272	37.57	11.37	2.318	44.38
2	8/25/2021	McKeil Pt a	0.505	26.58	2.10	0.496	25.88
3	8/25/2021	McKeil Pt b	0.825	43.02	1.54	0.745	40.14
4	9/17/2021	Susquehanna Pt a	1.956	10.12	0.72	1.844	10.32
5	9/17/2021	Susquehana Pt b	2.568	26.76	4.44	1.658	23.62
6	9/21/2021	Town Pt	0.586	9.13	0.40	0.408	8.61
7	9/21/2021	McKeil Pt	0.92	23.43	1.63	1.538	31.77

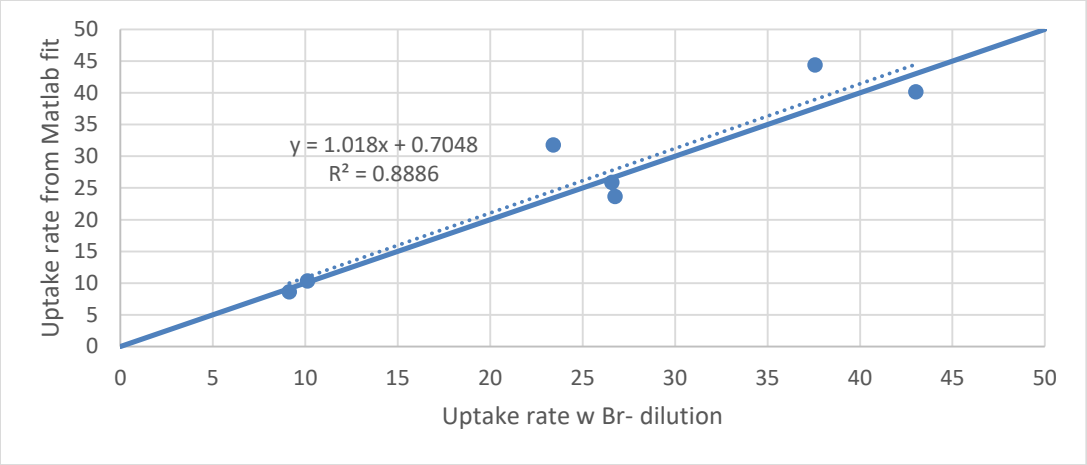

Figure 17. Plot of oxygen flux rates derived from equation 1.7 using bromide dilution rates, and by fit of the oxygen time course with the curvature of the time course yielding a dilution rate.

Results and Discussion

Operational Observations

Deploying the lander requires a sturdy davit and the ability to keep the boat in a location for ~1 hour. Similar to the Kellogg et al. (2013) tray methodology, this approach has limits in terms of days that are adequate for successful deployment or tray retrieval. In the Chesapeake Bay, the low overall tidal flows tend to keep the vessel in the same anchoring orientation without presenting difficulties with anchoring. However, wind, especially variable wind, in combination with tide can make some days difficult for deployment. From an operational viewpoint, there is a need to establish "windows" for sampling, rather than assign days too far in advance.

Leakage Estimates

At the outset of the project, we evaluated both rhodamine dye and bromide as tracers of leakage due to the incomplete seal of the chamber to the bottom due to oyster-derived small scale topography. Although rhodamine proved to be a good tracer of mixing in the chamber using filtered water in a laboratory setting, but adsorption of rhodamine to particulates, both in the benthos and suspended in the water column, this was especially noted when samples were filtered and the particulates were stained with rhodamine.

Bromide showed a strong exponential decrease in all cases (Figure 15, Figure 18). The added or excess bromide in the sample was used as the tracer, with the bromide background subtracted. Similar decay coefficients were determined for all 13 data points (0.923 h^{-1}), 7 data points (0.949 h^{-1}) and 4 data points (0.986 h^{-1}), suggesting that fewer data points, with a likely constant leakage rate, may be adequate.

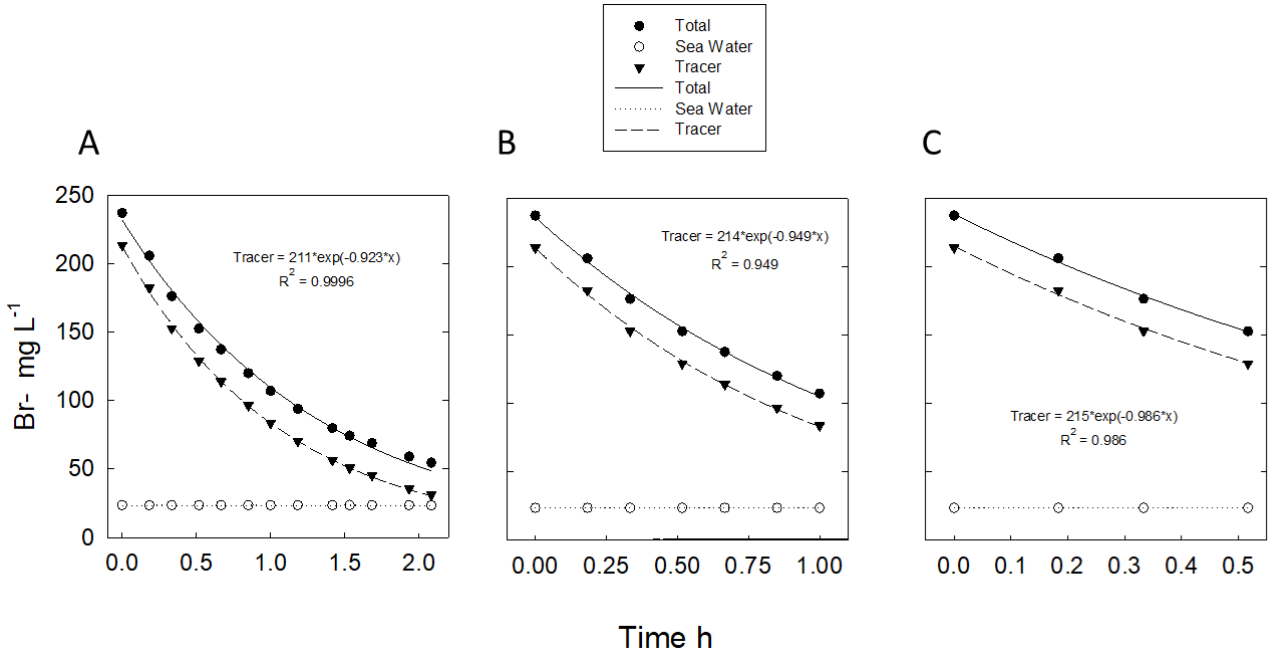

Figure 18. September 21, 2021 McKeil Point bBromide time course showing total bromide, added bromide and "background" bromide from brackish water. Plot A is for > 2 hours, plot B is for 1 h, and plot C is for 0.5 h.

The rate of bromide disappearance is dependent on site characteristics, such as the small scale topographic vertical changes related to the distribution and orientation of oysters and oyster shell. Using the same site coordinates at McKeil Point, and recognizing that our deployment location could change on the ~10-20 m spatial scale, we observed a wide range of dilution rates. The lowest rate suggested that ~1/2 of the water was diluted via leakage, while the highest rate suggested that water was replaced ~2.5 times within one hour. The data suggest that a broad range of leakage rates are to be expected in a restored oyster reef.

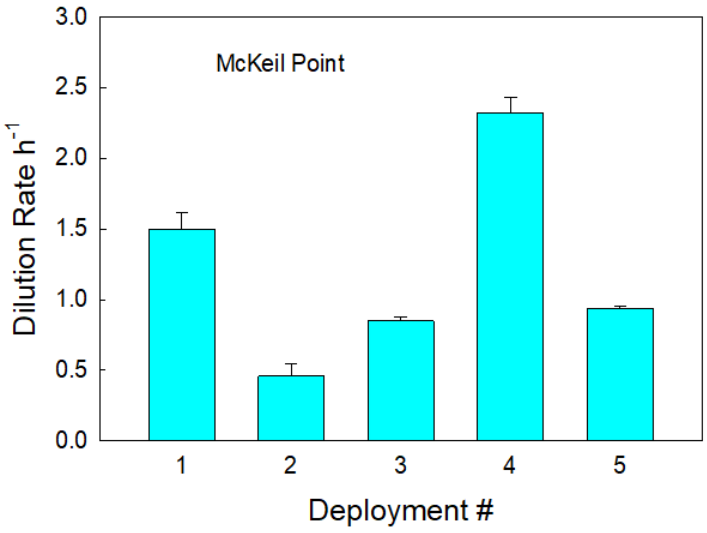

Figure 19. Rate of leakage for 5 lander deployments on multiple dates at McKeil Point in 2021.

While the most direct way to measure leakage is changes in excess bromide, it should be noted that in many cases we were able to detect the added bromide in the sensor data for conductivity. Figure 20A shows the change in concentration of Br- with a leakage of 1.26 h^{-1}. Although the added Br^- only changed the total conductivity 1.1%, the estimate for leakage is relatively similar to the Br- calculation (1.42 h^{-1}). This suggests that adding conductivity, even by added a modest amount of salt to increase salinity, likely can provide the dilution data necessary for making flux calculations. The chief caveat is that in estuarine systems in which observed salinity changes over time due to tides, the signal must be sufficient to not be rendered useless. Several of our conductivity time courses exhibited short-term exponential behavior, confounded by subsequent changes that did not fit the dilution model. However, adding 1 psu salinity in the Little Choptank would not have physiological or microbial effects on the benthic community and would 1) eliminate the need for the relatively expensive bromide analysis, 2) greatly improve the signal to noise in the "excess"conductivity estimate, 3) provide many more data points for curve fitting, and 3) provide field data sufficient to quickly estimate oxygen uptake under conditions of chamber leakage. This approach needs more comparisons to bromide-derived leakage estimates.

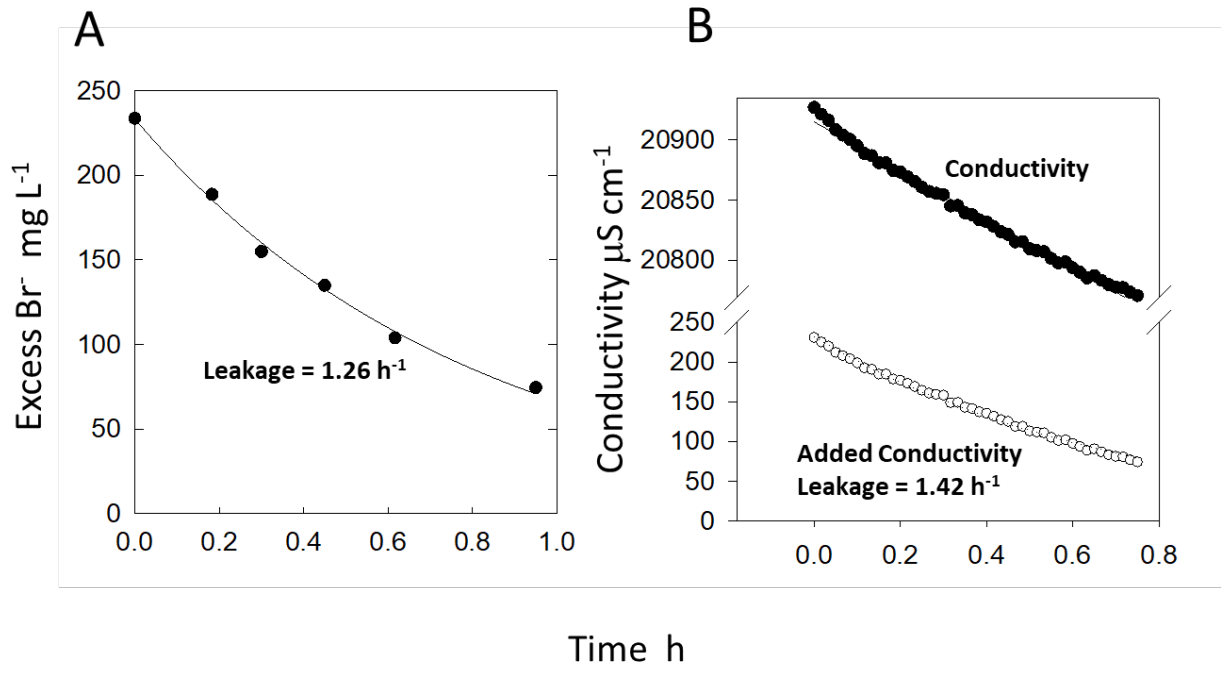

Figure 20. Leakage data from Susquehanna Point (8/20/2021). Panel A shows the bromide change over time and panel B shows changes in total conductivity and changes in the conductivity from the added bromide.

Oxygen Time Courses and Fluxes

The calculation of oxygen uptake is described previously and will not be discuss here. Figure 21 shows all of the oxygen time courses and show instances with a strong approach to asymptotic concentrations (example 4 and 7), some cases in which oxygen decreases at a rapid rate over time (examples 2 and 3). It is important to note that the total oxygen depletion always leaves > 50% of the original concentration, potentially alleviating artifacts associated with low oxygen such as changing behavior of different animal species, decreased oxygen penetration into sediment, and decreased nitrification. (Owens and Cornwell 2020).

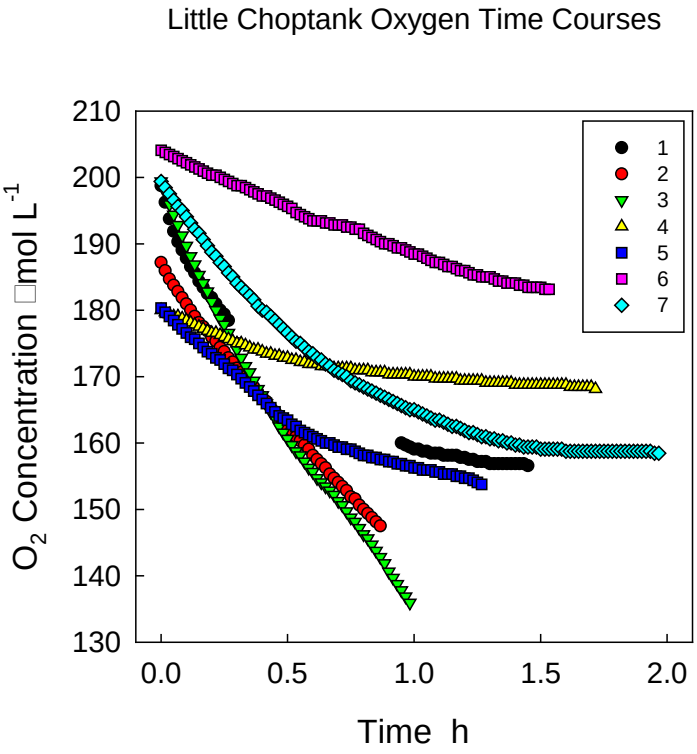

Figure 21. Field oxygen concentrations plotted over time. The numbers correspond to the deployments shown in Table 3.

Nutrient Fluxes and Denitrification

Although equation 1.7 can be applied to the estimation of individual nutrient exchange rates, the lower number of data points relative to the field oxygen measurements makes that approach less robust. In addition, the small changes in nutrient concentrations can amplify the effect of normal analytical variation.

The approach used here is to look at the relationship between the nutrient concentration over time and the discrete gas sample colected simultaneously and analyzed later on the mass spectrometer (Kana et al. 1994) for both oxygen and nitrogen concentrations. Thus, denitrification can be calculated via examination of the slope of the N_2/O2 relationship, multiplying that slope by the oxygen flux calculated from sensor data to get a net flux (eq. 1.8). The N_2 flux is multiplied by 2 to get the N flux. The calculation for dissolved ammonium, nitrate+nitrite, and soluble reactive P is done in a similar fashion but without multiplication by 2 (eq. 1.9).

$$N_2\text{-N Flux} = O_2\text{Flux}_{(YSI)} * \Delta N_2/\Delta O_{2(\text{mass spec})} * 2 \quad (1.8)$$

$$NH_4^+ \text{ Flux} = O_2\text{Flux}_{(YSI)} * \Delta NH_4^+/\Delta O_{2(\text{mass spec})} \quad (1.9)$$

A key advantage of this approach is that the rate is dependent on multiple points in a linear regression and can result in the use of appropriate statistical tests to examine the data set for significance of the slope. Figures 22-33 show the time course data for nutrients and the data as a function of oxygen concentration. Tables 4-7 show the slope of the relationship, the significance of the slope, and the estimate of nutrient fluxes based on equations 1.8 and 1.9.

Ammonium Fluxes

During the course of the incubations, ammonium concentrations increased a total of 1-2 to > 8 μmol L^{-1} (Figure 22). While several incubations appeared quite linear over time (e.g. incubations 1, 3, 6), some appeared to have some asymptotic shapes (incubations 4, 7). When plotted against oxygen concentrations (Figure 23) the data appear to have linear behavior for at least a number of points. Some data points appear more spurious (the highest ammonium concentration in plot 2), other plots have a lot of variability at lower oxygen concentrations, generally towards the end of the incubation, and some plots have too few points to make any judgment about linear character (plot 5).

Linear regression of the ammonium-oxygen data (Figure 24) yielded significant ($P < 0.05$) slopes of the relationship, ranging from 0.03 to 0.14, with only 1 non-significant relationship (incubation 5). The R^2 valuses were generally 0.91 or better. The resultant NH_4^+ fluxes ranged from 0.6 to 5.9 mmol m^{-2} h^{-1}, the latter being an exceptionally high rate. McKeil Point incubations generated high (1.5-5.9 mmol m^{-2} h^{-1}) rates of NH_4^+ efflux.

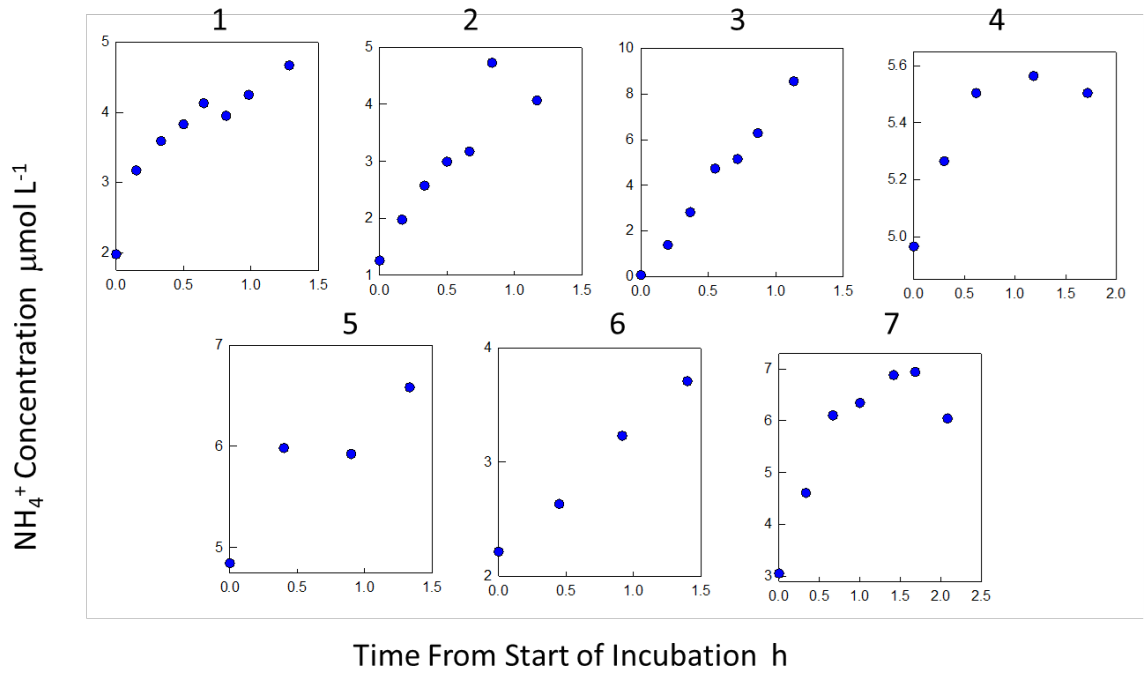

Figure 22. Time courses of ammonium concentration. The plot ID's (1-7) correspond to the data in Table 4.

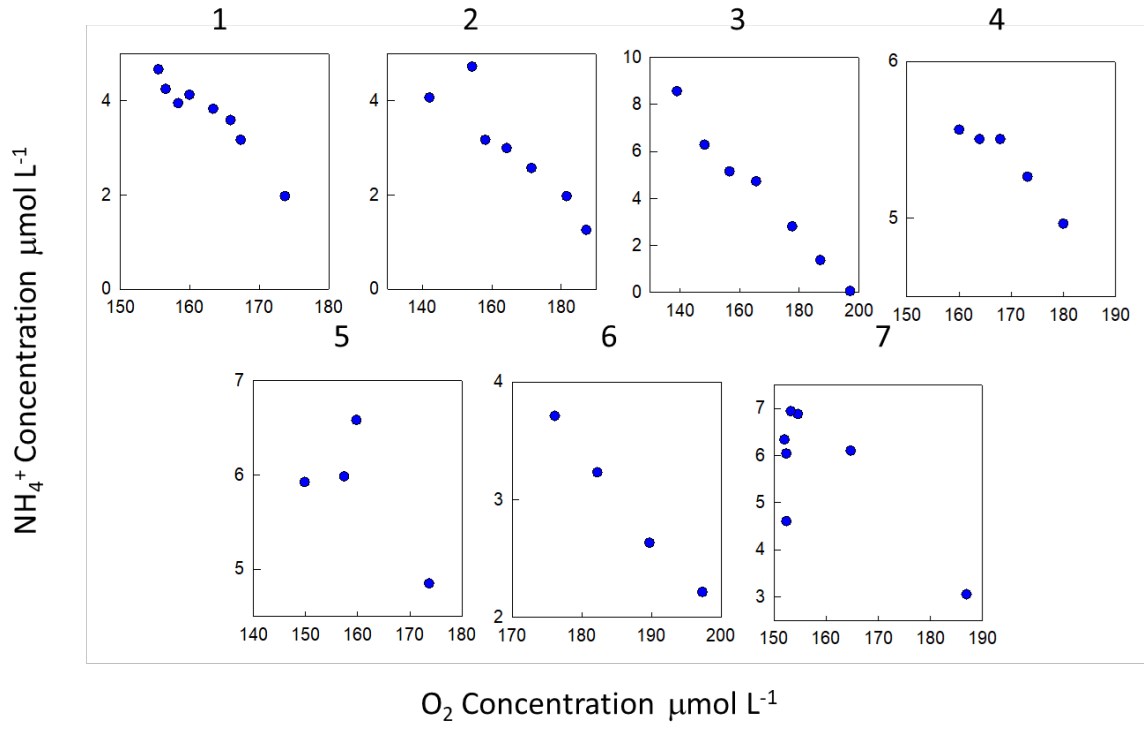

Figure 23. Plot of all ammonium data versus the corresponding oxygen concentrations derived from O_2/Ar measurements.

Table 4. Calculations for ammonium fluxes. For significance, we show orange shading for significance > 0.10.

	Site/Date	Slope	Slope Std Error	Intercept	R^2	P	O_2 Flux	NH_4^+-N Flux
		NH_4^+/O_2		µmol L^{-1}			mmol m^{-2} h^{-1}	
1	McKeil 8 20	0.1270	0.0157	24.4	0.917	< 0.001	37.57	4.77
2	McKeil 8 25	0.0589	0.0049	12.5	0.973	< 0.001	26.58	1.57
3	McKeil 8 25	0.1380	0.0080	27.2	0.974	< 0.001	43.02	5.94
4	Susquehanna 9 17	0.0304	0.0054	10.5	0.913	0.011	10.12	0.31
5	Susquehanna 9 17	0.0504	0.0369	13.9	0.483	0.305	26.76	1.35
6	Town Pt 9 21	0.0713	0.0042	16.2	0.993	0.005	9.13	0.65
7	McKeil 9 21	0.1170	0.0105	25.0	0.984	0.008	23.43	2.74

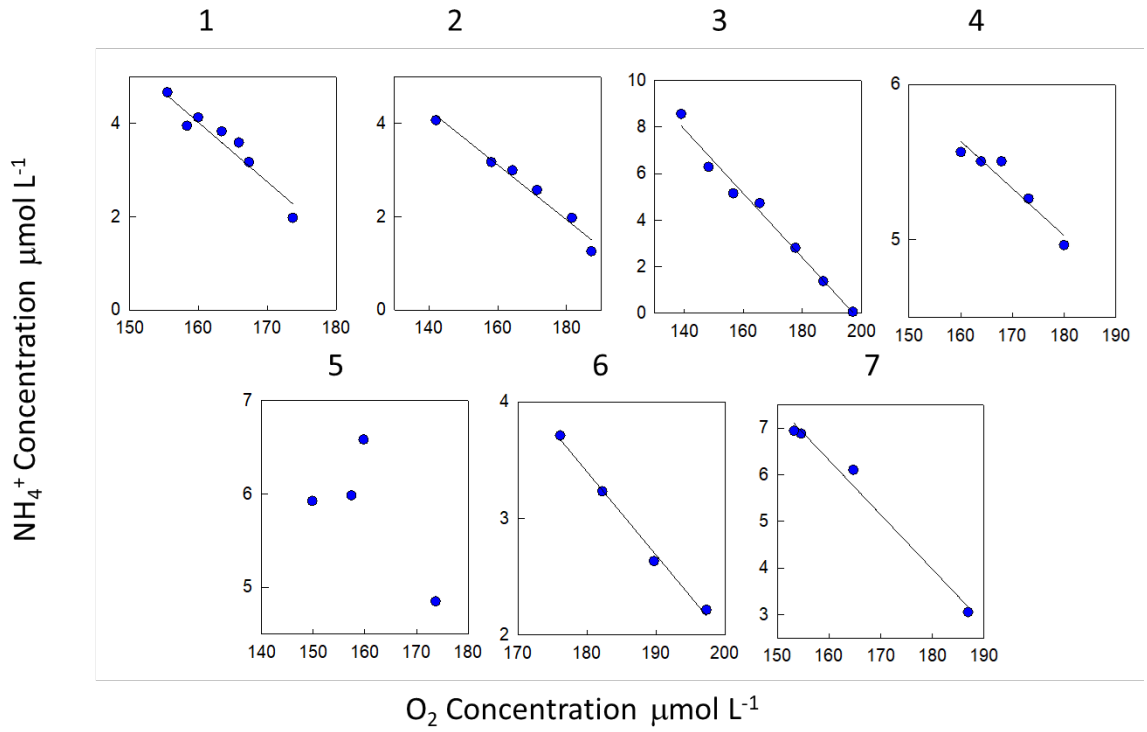

Figure 24. Plot of ammonium data used to estimate NH_4^+ to O_2 ratios. The lines are from linear regression and the slope and intercept are shown in Table 4.

Nitrate + Nitrite (NO_x^-) Fluxes

The concentrations of NO_x^- started at ~2-4 µmol L^{-1} and changed ~1 µmol L^{-1} in most cases (Figure 25). Complex time courses were observed in some cases (plot 7). Consequently, many of the O_2-NO_x^- plots exhibited a lot of variability (Figure 26). With the removal of some apparently spurious points, regressions had significant slopes with $P < 0.05$ for two plots and two plots with higher P values that remained under 0.1 (Table 5, Figure 27).

Relative to ammonium, the NO_x^- data is not a robust, at least partly because of the low dynamic range. The NO_x^- analysis has a reproducibility of ~0.07 µmol L^{-1} (Garcia-Robledo et al. 2014) and the small changes observed in some incubations may be difficult to discern due to the sensitivity of the analysis. The early McKeil incubations (1-3) suggest an efflux of ~ 1 mmol m^{-2} h^{-1}. Though not significant, it is clear that the small changes in other incubations would result in much lower rates than 1 mmol m^{-2} h^{-1}.

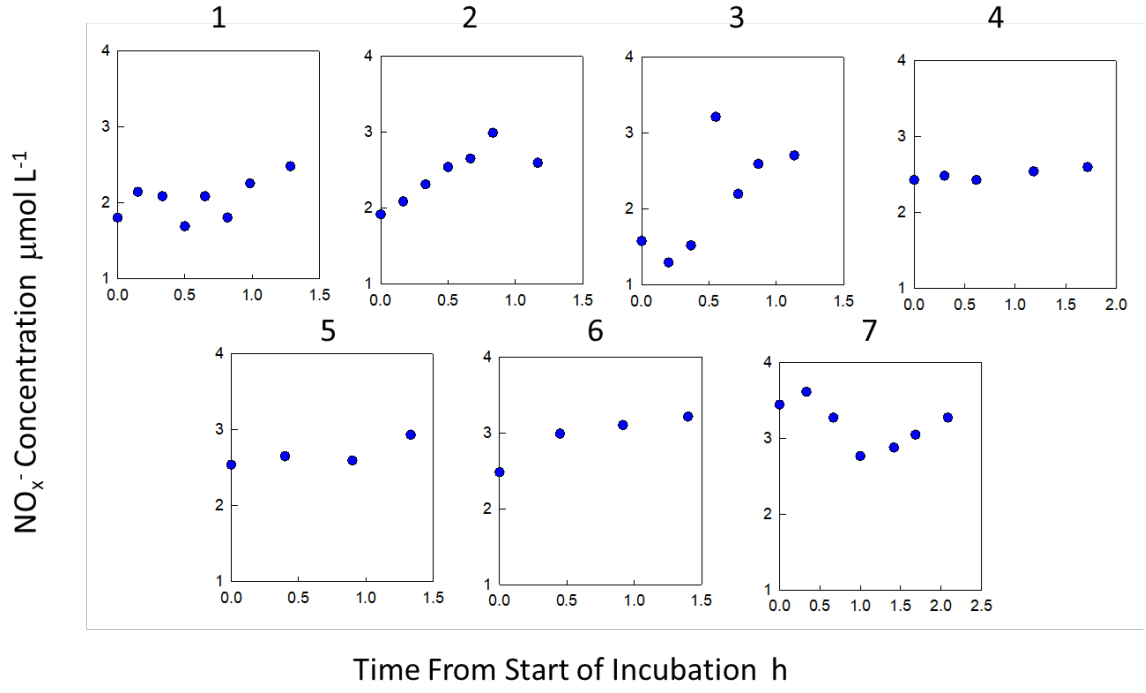

Figure 25. Time courses of NO_x^- (nitrate + nitrite) concentration. The plot ID's (1-7) correspond to the data in Table 5.

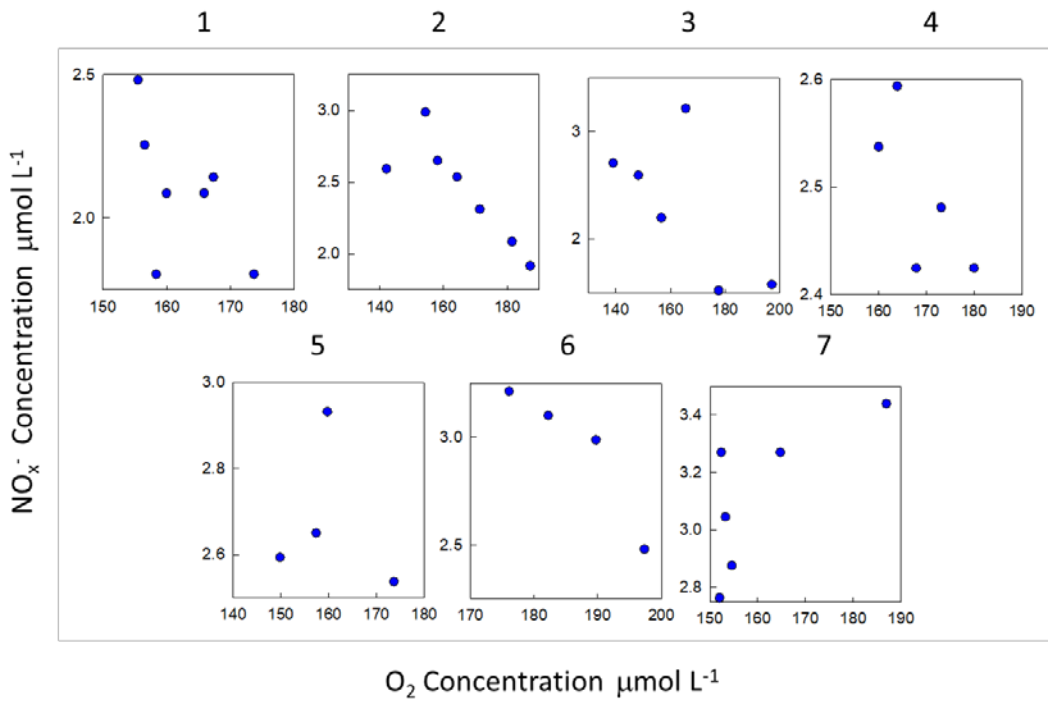

Figure 26. Plot of all NO_x^- data versus the corresponding oxygen concentrations derived from O_2/Ar measurements.

Table 5. Calculations for NO_x^- fluxes. For significance, we show orange shading for significance > 0.10 and yellow shading for significance between 0.005 and 0.10.

	Site/Date	Slope	Slope Std Error	Intercept	R^2	P	O_2 Flux	NO_x^- Flux
		NO_x^-/O_2		µmol L^{-1}			mmol m^{-2} h^{-1}	
1	McKeil 8 20	0.0322	0.0118	7.5	0.553	0.035	37.57	1.21
2	McKeil 8 25	0.0195	0.0055	5.7	0.719	0.016	26.58	0.86
3	McKeil 8 25	0.0251	0.0103	6.4	0.544	0.058	43.02	1.08
4	Susquehanna 9 17	0.0067	0.0038	3.6	0.504	0.179	10.12	0.07
5	Susquehanna 9 17	0.0036	0.0122	3.2	0.041	0.798	26.76	0.09
6	Town Pt 9 21	0.0329	0.0088	9.1	0.874	0.065	9.13	0.30
7	McKeil 9 21	-0.0033	0.0079	2.8	0.055	0.704	23.43	-0.08

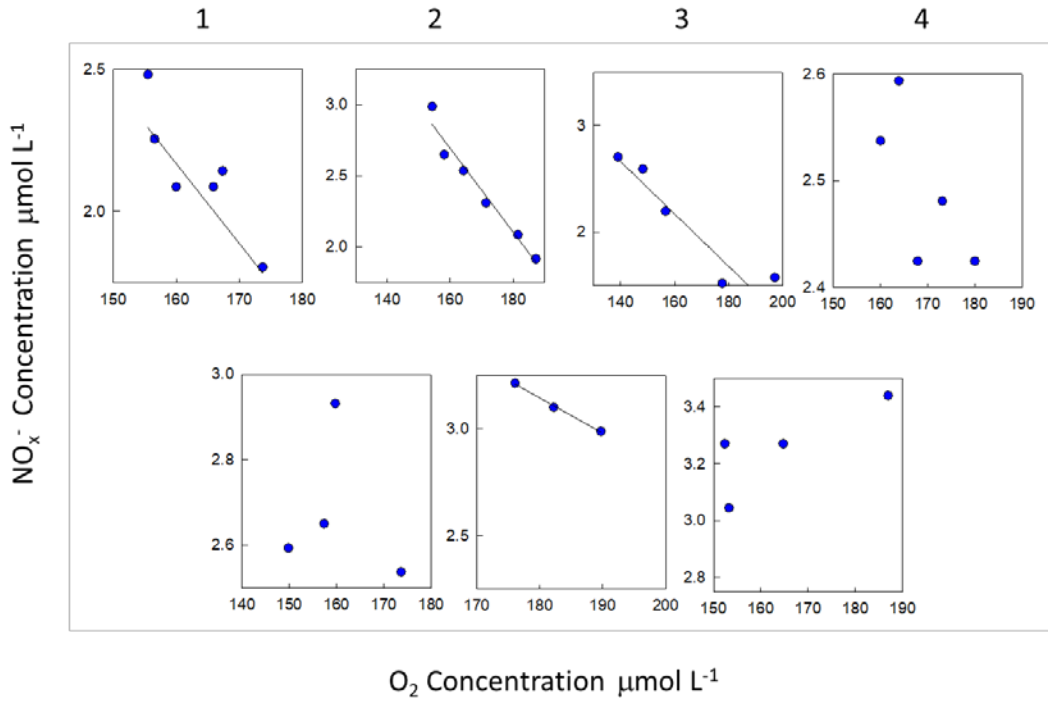

Figure 27. Plot of NO_x^- data used to estimate NO_x^- to O_2 ratios. The lines are from linear regression and the slope and intercept are shown in Table 5.

Di-Nitrogen (N_2) Fluxes

The time course of N_2 data is presented in Figure 28 and relative to the other nutrient fluxes, starts at a very high concentration due to the inherent solubility of N_2, the dominant atmospheric gas. The amount of change was typically 1-3 µmol L^{-1}. The reproducibility of the N_2/Ar approach is ~0.01-0.02%; for a N_2 concentration of 450 µmol L^{-1}, that translates into a sensitivity of 0.045 to 0.09 µmol L^{-1}, or a signal to noise ratio for this level of change of 10-66. This level of more than sufficient to make flux calculations.

Interpretable increases in the N_2 as a function of oxygen were observed in most cases (Figure 28), with P values < 0.05 for plots except 5 and 7 (Figure 29; Table 6). Plot 7 had a P of 0.066; using the 3 linear points resulted in a significant slope and the same N_2-N flux rate, but is not shown. Rates of denitrification were generally high, with most rates between 1 and 3 mmol N m^{-2} h^{-1}. For the McKeil Point data, rates averaged 2.1 0.6 mmol N m^{-2} h^{-1}.

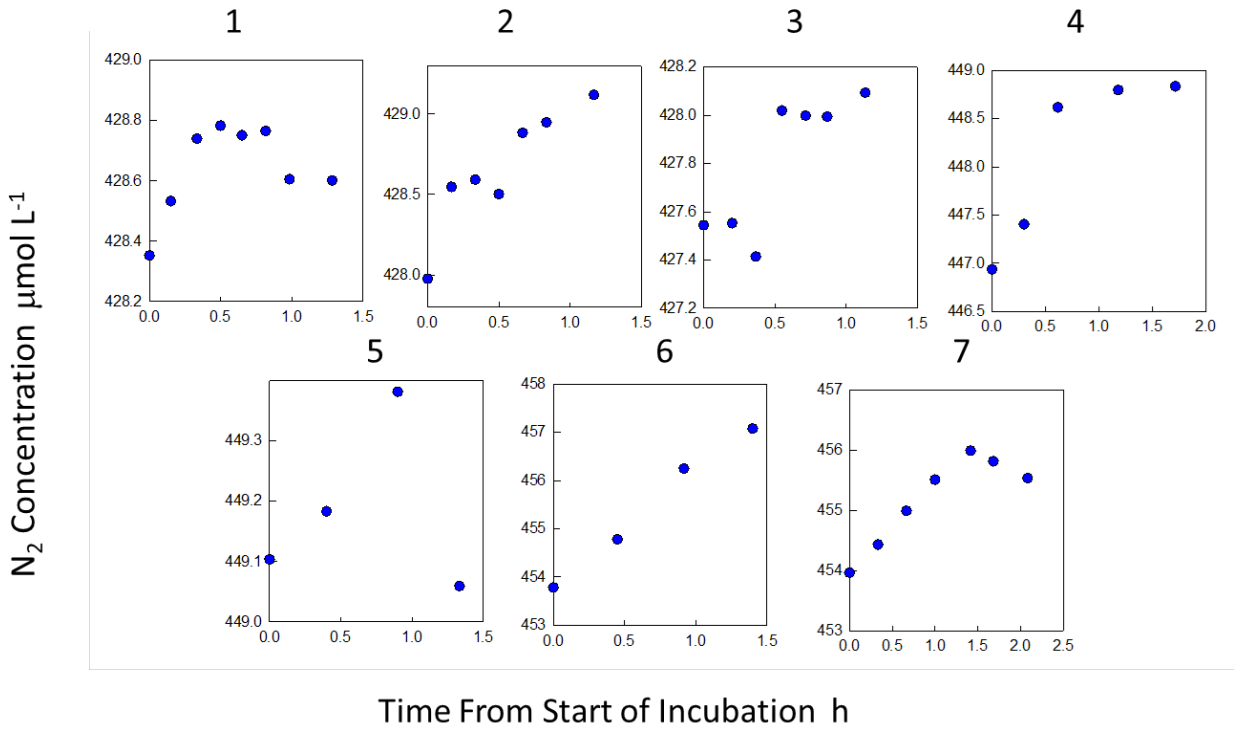

Figure 28. Time courses of N_2 concentration. The plot ID's (1-7) correspond to the data in Table 6.

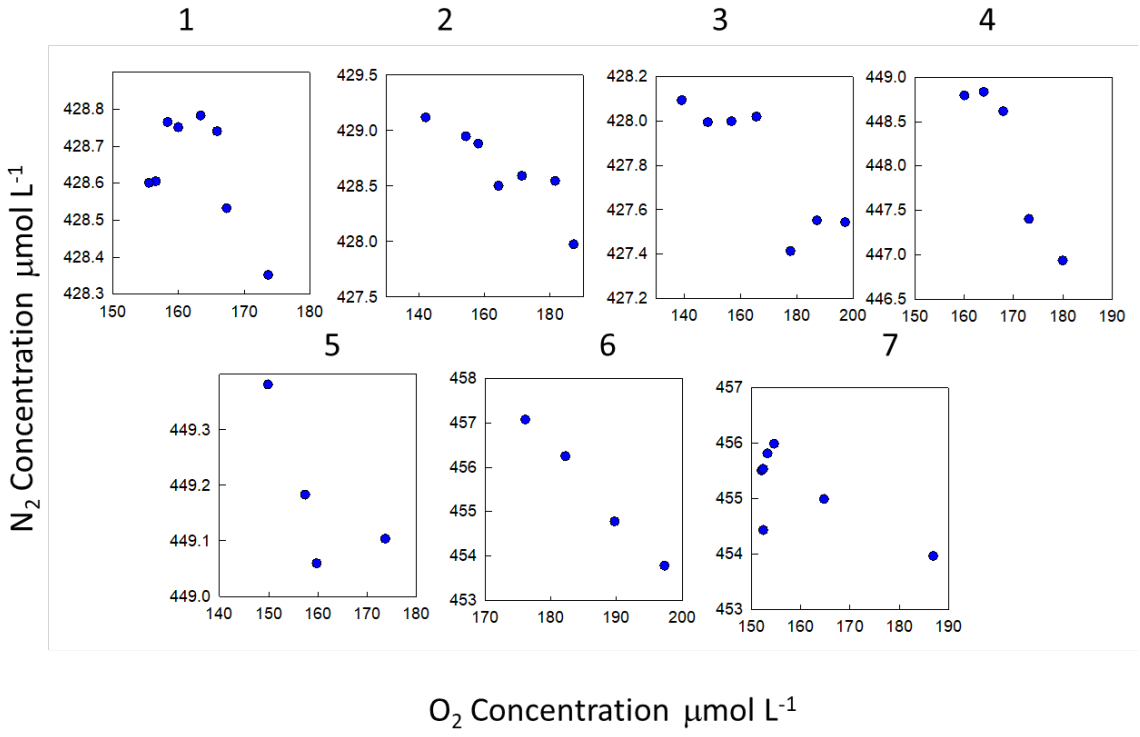

Figure 29. Plot of all N_2 data versus the corresponding oxygen concentrations derived for O_2/Ar measurements.

Table 6. Calculations for N_2-N fluxes. For significance, we show orange shading for significance > 0.10 and yellow shading for significance between 0.005 and 0.10.

	Site/Date	Slope	Slope Std Error	Intercept	R^2	P	O_2 Flux	N_2-N Flux
		N_2/O_2		$\mu mol\ L^{-1}$			$mmol\ m^{-2}\ h^{-1}$	
1	McKeil 8 20	0.0278	0.0073	433.2	0.782	0.019	37.57	2.09
2	McKeil 8 25	0.0218	0.0004	432.3	0.828	0.004	26.58	1.16
3	McKeil 8 25	0.0116	0.0031	429.7	0.741	0.013	43.02	1.00
4	Susquehanna 9 17	0.1070	0.0211	466.2	0.895	0.015	10.12	2.17
5	Susquehanna 9 17	0.0103	0.0070	450.8	0.521	0.278	26.76	0.55
6	Town Pt 9 21	0.1600	0.0092	485.2	0.993	0.003	9.13	2.92
7	McKeil 9 21	0.0419	0.0179	462.9	0.523	0.066	23.43	1.96

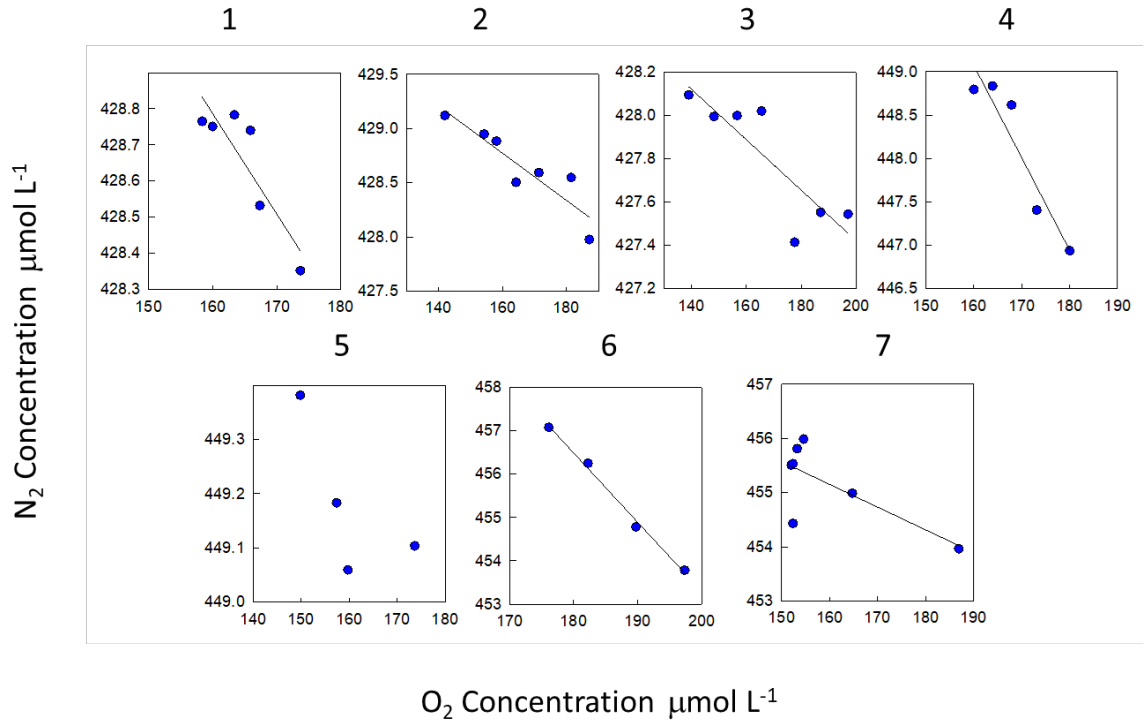

Figure 30. Plot of N_2 data used to estimate N_2 to O_2 ratios. The lines are from linear regression and the slope and intercept are shown in Table 6.

Soluble Reactive Phosphorus (SRP) Fluxes

Similar to the data for NO_x^-, the dynamic range of the SRP data is relatively small. Initial concentrations were < 0.25 µmol L^{-1}, with the highest concentrations at the end of the incubation approaching 0.5 µmol L^{-1} (Figure 31). Five of the 7 had increases in SRP that yielded useful changes in the SRP/O2 ratio (Figure 32), with two sites having negligible or zero changes in SRP (Plots 1, 6). The SRP flux rates ranged from 0 to 0.25 mmol m^{-2} h^{-1} with 4 sites having P < 0.05 (Figure 33, Table 7).

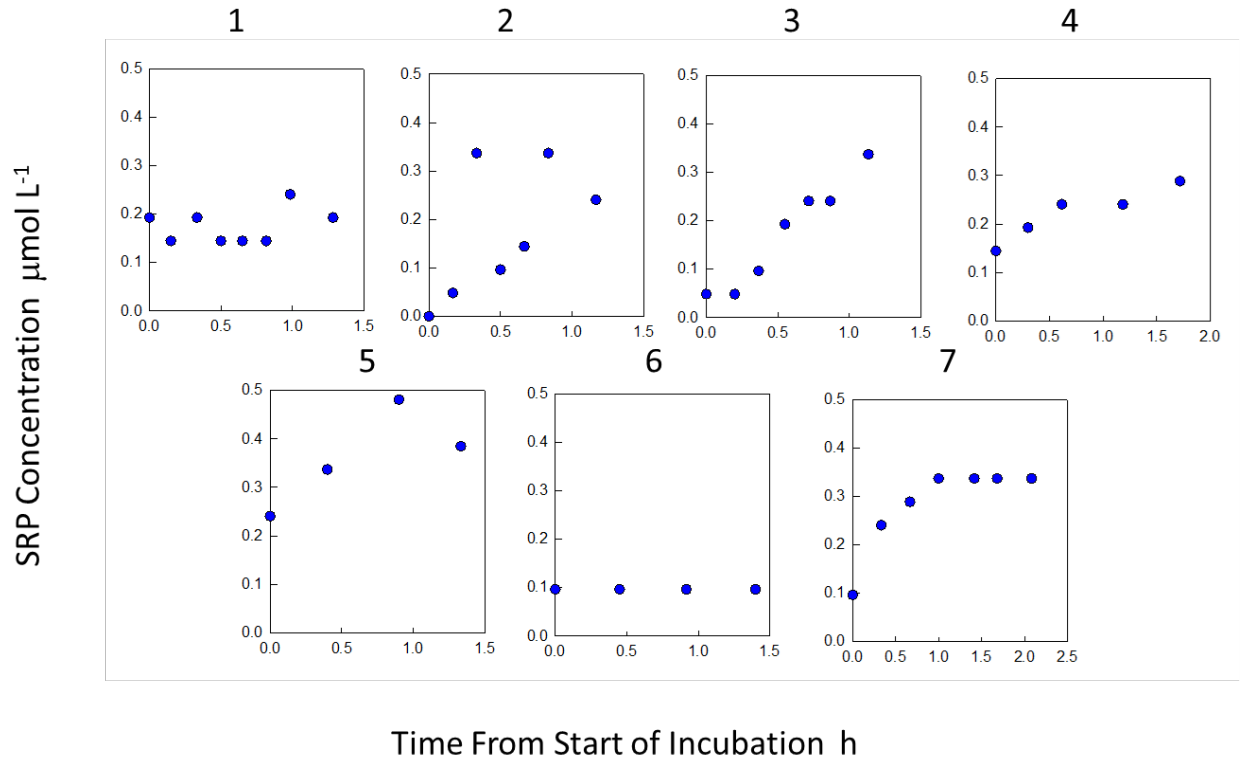

Figure 31. Time courses of SRP concentration. The plot ID's (1-7) correspond to the data in Table 7.

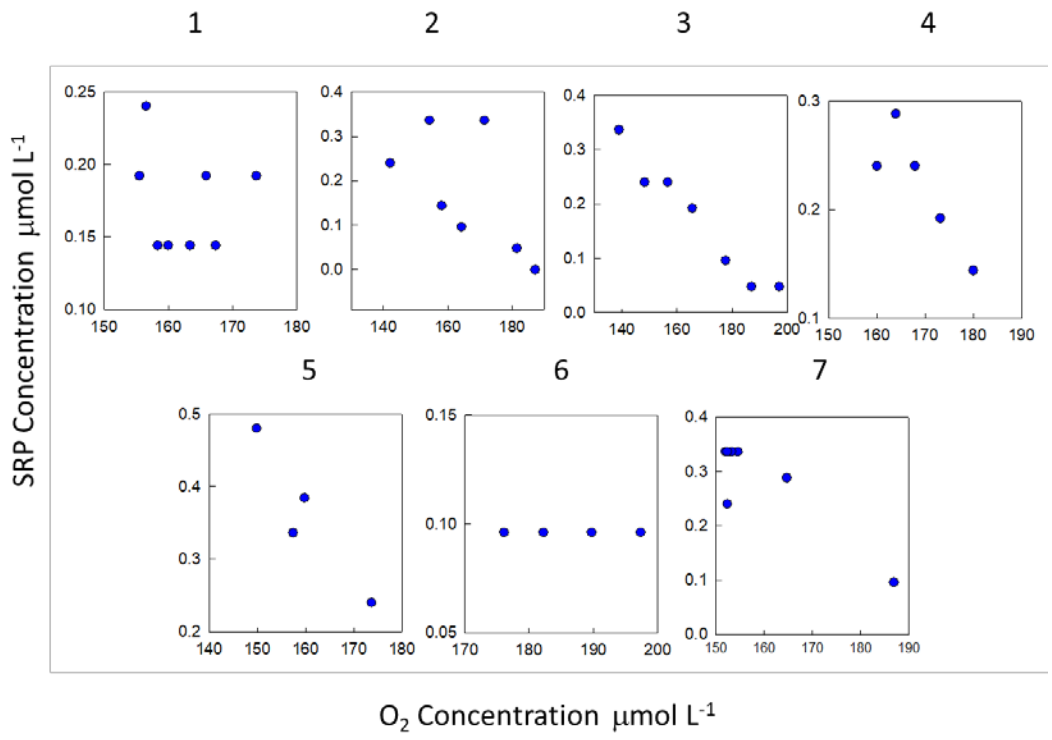

Figure 32. Plot of all SRP data versus the corresponding oxygen concentrations derived for O_2/Ar measurements.

Table 7. Calculations for SRP fluxes. For significance, yellow shading for significance between 0.005 and 0.10.

	Site/Date	Slope	Slope Std Error	Intercept	R^2	P	O_2 Flux	SRP Flux
		SRP/O_2		µmol L^{-1}			mmol m^{-2} h^{-1}	µmol m^{-2} h^{-1}
1	McKeil 8 20						37.57	0.000
2	McKeil 8 25	0.0050	0.0005	0.9	0.974	0.002	26.58	0.133
3	McKeil 8 25	0.0051	0.0005	1.0	0.954	< 0.001	43.02	0.220
4	Susquehanna 9 17	0.0079	0.0006	1.6	0.994	0.049	10.12	0.080
5	Susquehanna 9 17	0.0095	0.0024	1.9	0.884	0.060	26.76	0.253
6	Town Pt 9 21	0.0000	0.0000				9.13	0.000
7	McKeil 9 21	0.0007	0.0006	1.4	0.975	<0.001	23.43	0.016

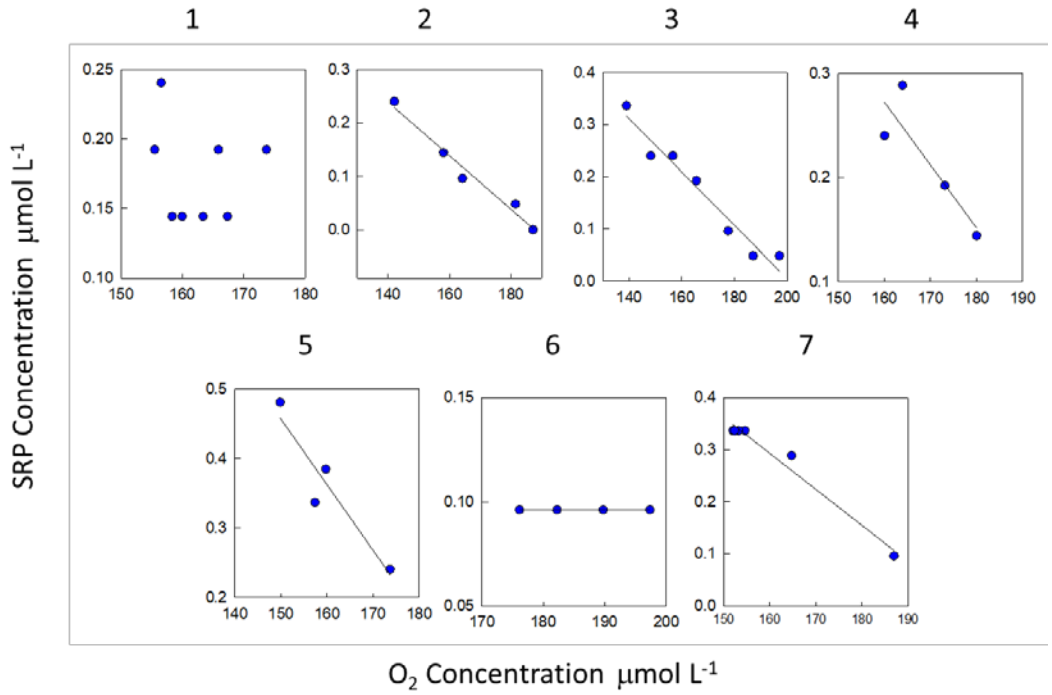

Figure 33. Plot of SRP data used to estimate SRP to O_2 ratios. The lines are from linear regression and the slope and intercept are shown in Table 7.

Little Choptank Denitrification and Nitrogen Fluxes

The flux data for nitrogen is summarized in Figure 34; non-significant flux rates are included in the stacked bars since most of the insignificant fluxes were low and changed the bar relatively little. It is clear that ammonium fluxes are a large part of the total flux of N, followed by N_2-N and NO_x^-. The highest total N corresponded to the high oxygen uptake rates.

The oxygen fluxes in the Little Choptank were higher than in Harris Creek (Figure 35), but somewhat lower than for the mid-Choptank site characterized by Kellogg et al. (2013). While the denitrification rates were higher than Harris Creek, they overlapped with the Kellogg data. The McKeil Point data ranged from 1-2 mmol N m^{-2} h^{-1}.

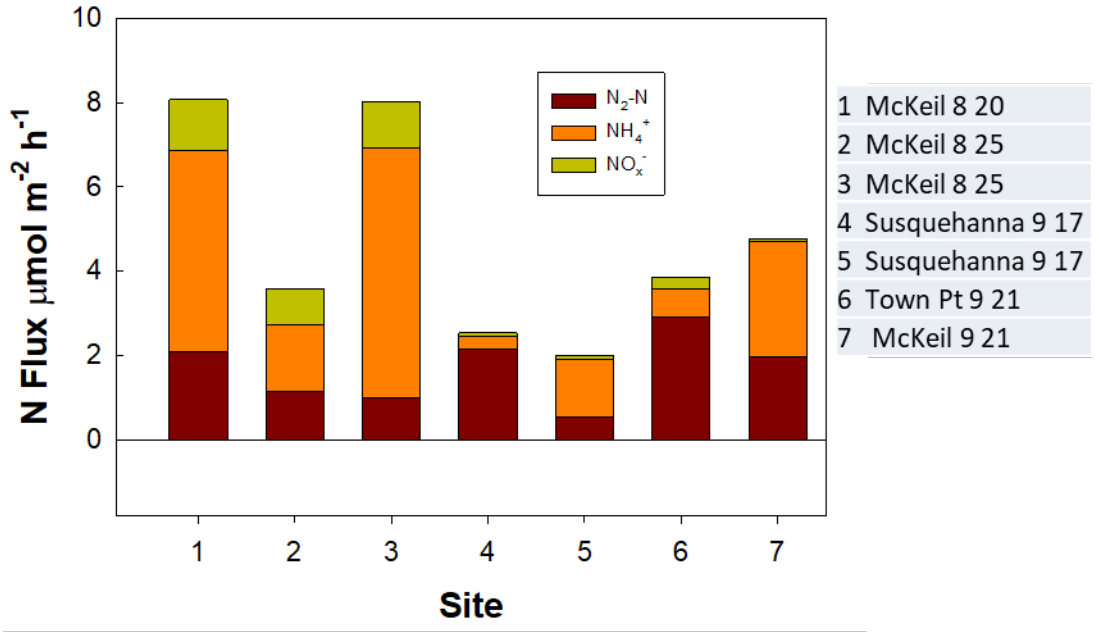

Figure 34. Stacked bar plot of all N fluxes. Note that some of the rates were not significant.

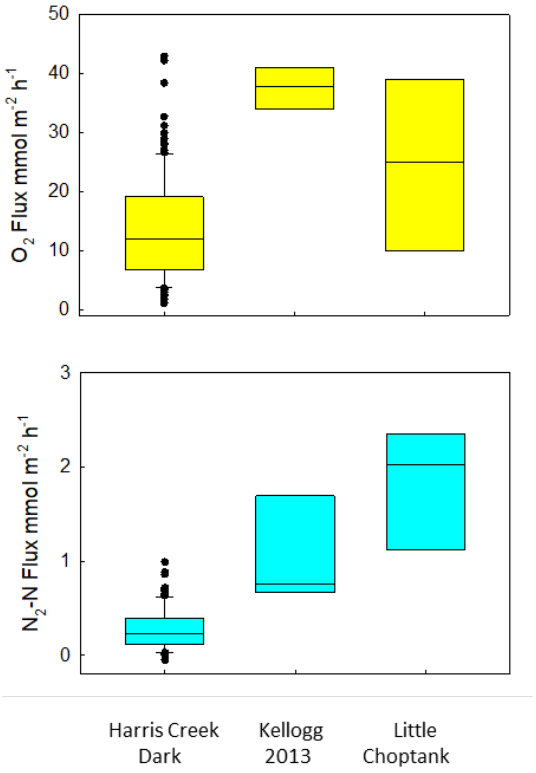

Figure 35. Box plots of oxygen fluxes and N_2-N fluxes from Harris Creek, a mid-Choptank site (Kellogg et al. 2013) and this study. The Harris Creek data is from summer and early fall, as is the Kellogg data.

One test of how reasonable these rates are is the use of nutrient regeneration stoichiometry. The expected ratio of C to N is 6.625 based on a Redfield algal stoichiometry and requiring terrestrial or macrophyte organic matter inputs are small. If we assume an oxygen to carbon ratio of ~1, as found in Kellogg et al. 2013, O_2 can be used as a proxy for C. If we take the sum of all N species from Figure 34 and plot them against oxygen (Figure 36)we can see if our data are "reasonable". For McKeil Point, the data fall well within the envelope of data from Kellogg et al. (2013) and Harris Creek. From these data, it appears that these high rates of nutrient remineralization and N_2 flux are reasonable. Two of the other Little Choptank observations appear to be outside the expected flux range and are suspect.

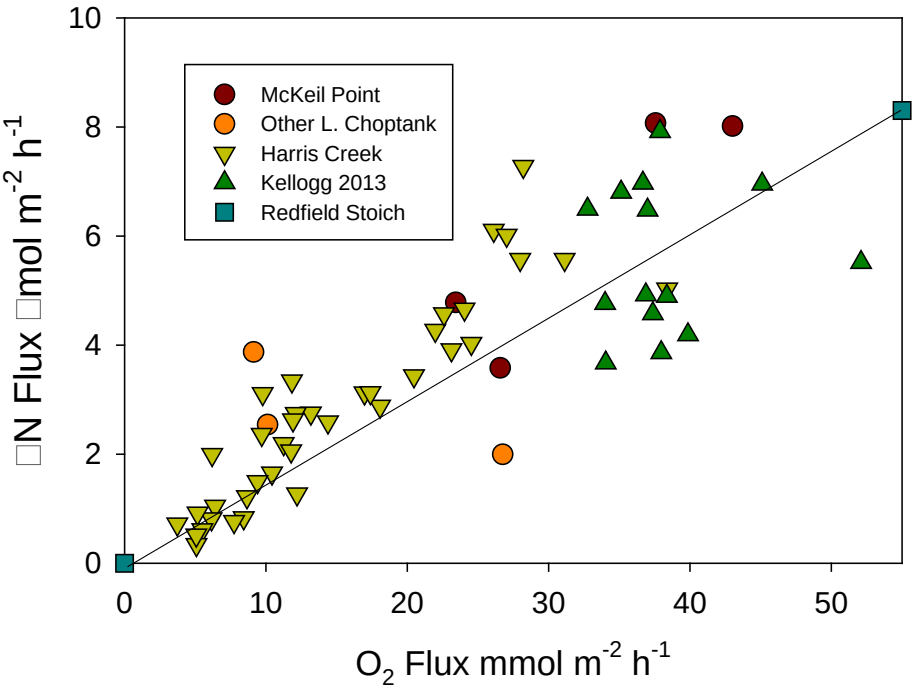

Figure 36. Plot of the sum of nitrogen flux species (NO_x^-, NH_4^+, N_2-N McKeil Point and other Little Choptank sites, summer and fall 2015 in Harris Creek, summer data from the upper Choptank (Kellogg et al. 2013), all compared to a plot of the expected ratio of total N remineralization to O_2 flux (0.151), assuming that O_2 reflects total carbon remineralization.

The data analysis from the ongoing BMP effort for oyster denitrification in restoration is being used to develop rates for crediting N removal via denitrification. The biomass of the summer data used for the analysis showed a lot of variability, with some denitrification rates approaching 0.5-1 mmol N m^{-2} h^{-1}. At the biomass measured in the Little Choptank, expected denitrification rates would be ~0.25 mmol N m^{-2} h^{-1}, considerably lower than observed in this study. We observed less inorganic sediment on top of the community in the Little Choptank, relative to the Harris creek data that is the dominant data source for Figure 37. These data, taken under conditions of less disturbance and lower biomass than the BMP analysis, suggest that at least in the Little Choptank, denitrification rates would be underestimated with current data analysis.

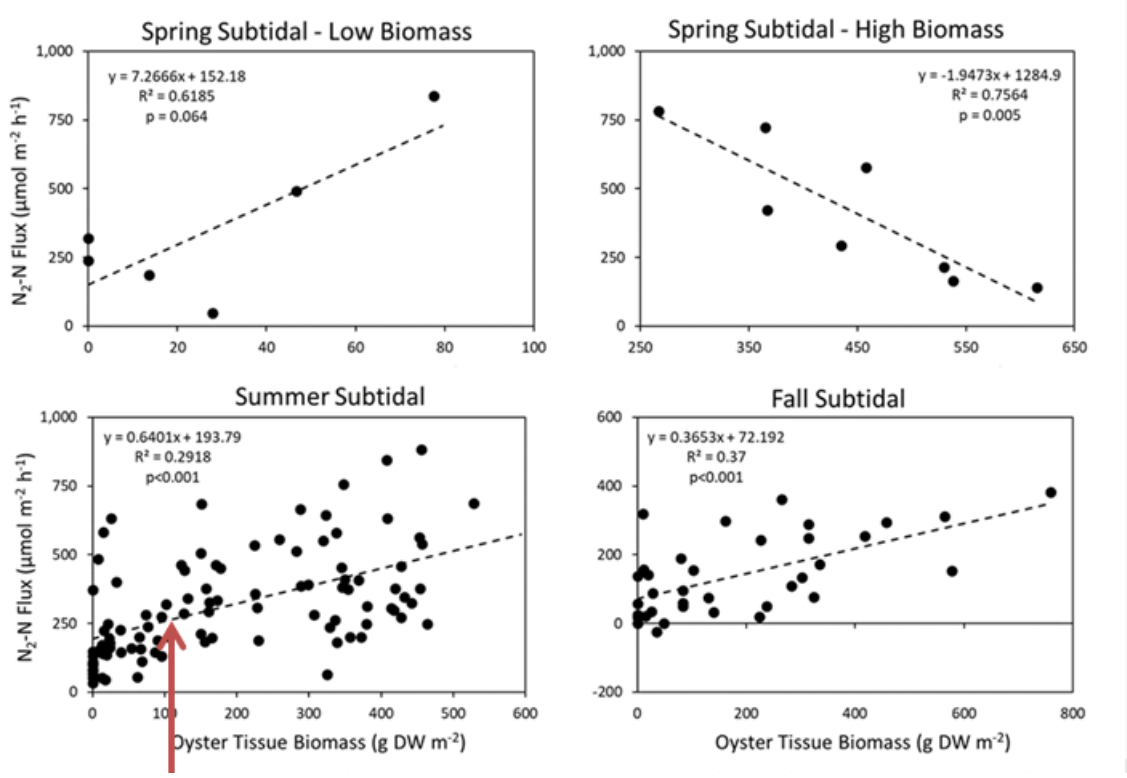

Figure 37. Biomass and denitrification relationship in oyster denitrification BMP (in progress). The red arrow shows the biomass at the Little Choptank sites, plotted on the summer subtidal plot. Data and figure were developed by Lisa Kellogg (VIMS).

Potential Improvements to Design and Operation

Although the deployments of the lander demonstrated the feasibility of the "leaky lander" approach, the experience of the research team naturally leads to suggestions to most efficiently deploy the system and interpret results. Several suggestions for consideration by future users are listed here:

1. A key lesson of this program is that the most valuable time course information occurs during the initial phase of oxygen decrease. In Figure 38, the most valuable oxygen and nutrient data is in the first half hour. If we consider a 23 µmol L^{-1} decrease in O_2, algal decomposition stoichiometry suggests that the production of 3.5 µmol L^{-1} of remineralized N. At 25% denitrification efficiency, that would be a 0.9 µmol L^{-1} increase in N_2-N, or ~0.1% of the N_2-N in the water. With a reproducibility of 0.02% for N_2-N, this modest decrease represents a signal to noise ratio of 5. With higher rates of oxygen depletion, the measurement of denitrification is even better constrained. Time points longer than ½ hour could be useful for estimating leakage, but provide only minimal gain in estimating oxygen and nutrient fluxes. Changing oxygen and nutrient concentrations in the water outside the chamber likely becomes more of an artifact in longer incubations.

2. The approach to using mop heads to help minimize exchange was used here because of its simplicity and low cost. Other solutions for minimizing leakage may improve upon this design.
3. The pumping system worked well for sampling, but in one instance it generated no usable N_2 and Ar data because cold water degassed within the pump tubing when the tubing above the water surface was heated on the boat deck. This can be alleviated by shorter lengths of tubing and/or keeping the tubing submerged in water on deck to maintain water temperatures.
4. The time course change of solutes and gases is a function of biogeochemical rates, rates of leakage, and lander height. A lander ½ of this system could have a much more change of concentration if the rates of leakage were not excessively high. If leakage rates are the same, it would mean that the oxygen decreases would have an asymptote at a much lower level of oxygen depletion.
5. Although illumination was present through the use of a clear acrylic lander top, the effects of light versus dark conditions would require use of shade material or an opaque cover. Alternatively, an underwater LED lighting system could be used. Although the general paradign of lower denitrification during illumination is suggested for sediments (Risgaard-Petersen 2003), work in oyster reefs do not show a substantial denitrification decrease with illumination (Cornwell et al. 2019).
6. Alternative mixing systems could be deployed. Underwater propellers from "toy" submarines may have promise for mixing; however, the pump approach used here is simple and mixes the entire chamber rapidly. The physics of the benthic boundary layer is , however, likely unrealistic and would require a very different approach (Porter et al. 2004).
7. The precision of estimation of oxygen fluxes is highly dependent on both the rate of oxygen depletion and upon the leakage rate. Figure 39 shows the standard error of estimation of oxygen flux plotted versus the leakage rate. It is clear that at high leakage, the ability to determine biogeochemical fluxes is much more difficult. Unfortunately, as shown in the high variability of leakage rate at a single site (Figure 19), the operator has no control over leakage. If leakage rates are excessive, there may be a need to reject data; this also implies that multiple deployments/high replication may be necessary to allow data rejection while still having a sufficient number of rates to characterize the system.

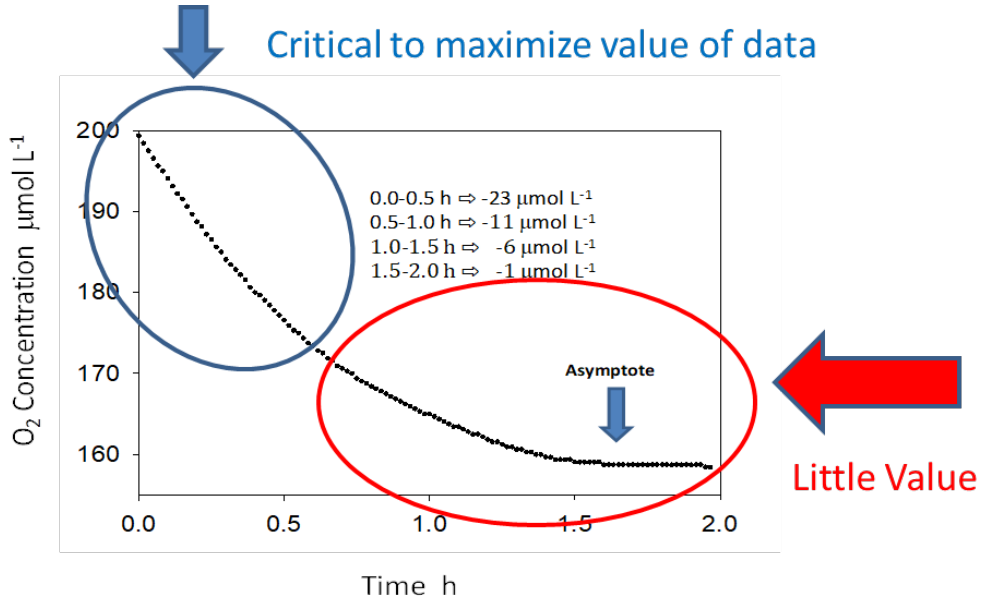

Figure 38. Time course of oxygen over ~ 2 hours. The data shown for showed a decrease of 23 µmol L^{-1} over the first half hour, 11 over the next half hour and only 7 over the next hour.

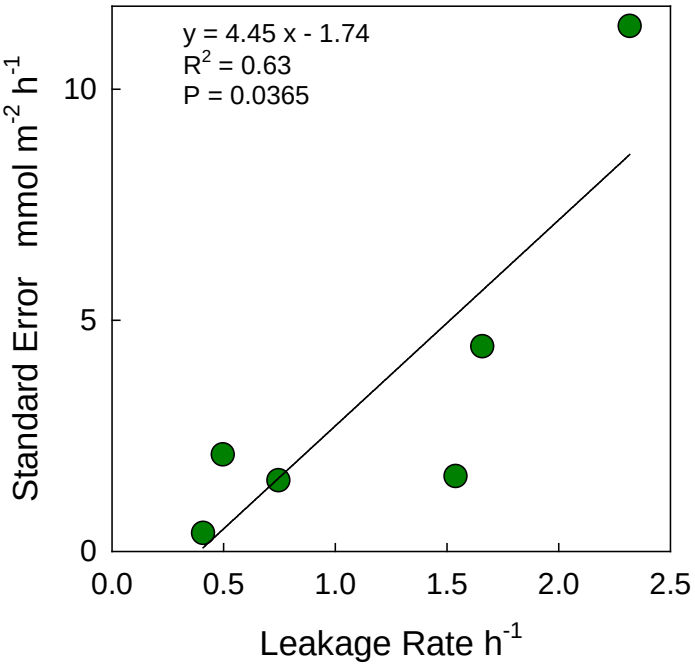

Figure 39. Plot of the standard error for estimated oxygen fluxes as a function of the leakage rate.

Acknowledgments

This work benefitted from guidance from the oversight panel chair, Dr. Suzanne Bricker, the panel members, and Sara Koser for assistance in identification of study sites in the Little Choptank River. Mr. Jack Seabrease from the HPL machine shop manufacture the lander and provided key advice during its construction. Finally, we are grateful to the Chesapeake Bay Trust for supplying this funding and for their patience after a late start on the project after a delay in getting the funding set.

References

Boynton, W. R., W. M. Kemp, C. G. Osborne, K. R. Kaumeyer, and M. C. Jenkins. 1981. Influence of water circulation rate on in situ measurements of benthic community respiration. Marine Biology **65**:185-190.

Bruce, D. G., J. C. Cornwell, L. Harris, T. F. Ihde, M. Lisa, S. K. Kellogg, R. N. Lipcius, D. N. McCulloch-Prosser, S. P. McIninch, and M. B. Ogburn. 2021. A Synopsis of Research on the Ecosystem Services Provided by Large-Scale Oyster Restoration in the Chesapeake Bay.

Cornwell, J. C., W. M. Kemp, and T. M. Kana. 1999. Denitrification in coastal ecosystems: environmental controls and aspects of spatial and temporal scale. Aquatic Ecology **33**:41-54.

Cornwell, J. C., M. S. Owens, W. R. Boynton, and L. A. Harris. 2016. Sediment-Water Nitrogen Exchange along the Potomac River Estuarine Salinity Gradient. Journal of Coastal Research **32**:776-787.

Cornwell, J. C., M. S. Owens, M. Jackson, and M. L. Kellogg. 2019. Integrated assessment of oyster reef ecosystem services: quantifying denitrification rates and nutrient fluxes. Final report to NOAA Chesapeake Bay Office, UMCES Technical Report TS-732-19.

Fisher, T. R., P. R. Carlson, and R. T. Barber. 1982. Sediment nutrient regeneration in three North Carolina estuaries. Estuarine, Coastal and Shelf Science **14**:101-116.

Garcia-Robledo, E., A. Corzo, and S. Papaspyrou. 2014. A fast and direct spectrophotometric method for the sequential determination of nitrate and nitrite at low concentrations in small volumes. Marine Chemistry **162**:30-36.

Jackson, M., M. S. Owens, J. C. Cornwell, and M. L. Kellogg. 2018. Comparison of methods for determining biogeochemical fluxes from a restored oyster reef. Plos One **13**:e0209799.

Kana, T. M., C. Darkangelo, M. D. Hunt, J. B. Oldham, G. E. Bennett, and J. C. Cornwell. 1994. Membrane inlet mass spectrometer for rapid high-precision determination of N_2, O_2, and Ar in environmental water samples. Analytical Chemistry **66**:4166-4170.

Kellogg, M. L., J. C. Cornwell, M. S. Owens, and K. T. Paynter. 2013. Denitrification and nutrient assimilation on a restored oyster reef. Marine Ecology Progress Series **480**:1-19.

Kellogg, M. L., A. R. Smyth, M. W. Luckenbach, R. H. Carmichael, B. L. Brown, J. C. Cornwell, M. F. Piehler, M. S. Owens, D. J. Dalrymple, and C. B. Higgins. 2014. Use of oysters to mitigate eutrohication in coastal waters. Estuarine Coastal and Shelf Science **151**:126-168.

Owens, M. S., and J. C. Cornwell. 2016. The Benthic Exchange of O-2, N-2 and Dissolved Nutrients Using Small Core Incubations. Jove-Journal of Visualized Experiments.

Owens, M. S., and J. C. Cornwell. 2020. Temporal enhancement of denitrification in bioirrigated estuarine sediments. Aquatic Sciences **82**:1-12.

Owens, M. S., S. P. Kelly, T. A. Frankovich, D. T. Rudnick, J. W. Fourqurean, and J. C. Cornwell. 2021. Controls on Nutrient Cycling in Estuarine Mangrove Lake Sediments. Journal of Marine Science and Engineering **9**:626.

Parsons, T. R., Y. Maita, and C. M. Lalli. 1984. A Manual of Chemical and Biological Methods for Seawater Analysis. Pergamon Press, New York.

Porter, E. T., L. P. Sanford, G. Gust, and F. S. Porter. 2004. Combined water-column mixing and benthic boundary-layer flow in mesocosms: key for realistic benthic-pelagic coupling studies. Marine Ecology-Progress Series **271**:43-60.

Risgaard-Petersen, N. 2003. Coupled nitrification-denitrification in autotrophic and heterotrophic estuarine sediments: On the influence of benthic microalgae. Limnology and Oceanography **48**:93-105.

Rose, J. M., S. B. Bricker, M. A. Tedesco, and G. H. Wikfors. 2014. A Role for Shellfish Aquaculture in Coastal Nitrogen Management. Environmental Science & Technology **48**:2519-2525.

Appendix I. Materials List

			#	Total Cost
Best Estimate Oct 2021 - single deployable chamber		Unit cost	Sum	$7,225.23
CHAMBER CONSTRUCTION				
mop replacement head	Amazon spin micro fiber mop	$3.17	9	$28.53
bilge pump for water circulation	Amazon: Johnson pump 500 gph	$37.64	1	$37.64
24" White PVC Schedule 40 pipe	We bought 14' for $100 per foot from our hatchery. US plastics current cost is $205.64 per foot, 20' minimum.	$100.00	2	$200.00
Acrylic top				
Aluminum angle for oyster tub		$12.40	1	$12.40
battery for bilge pump circulator	Amazon: Dakota lithium 12v 18 ah	$179.99	1	$179.99
Luer bulkhead fitting		$1.00	2	$2.00
lifting rings, handles, rope		$100.00	1	$100.00
battery for circulation pump	Amazon, Dakota lithium	$179.99	1	$179.99
acrylic sheet for top	Material was on hand, costo fo 12 mm 24" x 24" US Plastics	$69.91	1	$69.91
low voltage wire		$10.00	1	$10.00
tubing		$0.27	40	$10.80
Total chamber Cost				$820.46
SAMPLING APPARATUS				
peristaltic sampling pump	Dyrabrest 0-140 mL	$119.00	1	$119.00
case for pump storage	Amazon: Sheffield 12626 field box	$14.99	1	$14.99
ammeter to determine if pump is work	Amazon: Bediffer	$24.58	1	$24.58
battery pack for peristaltic sampling pu	Amazon: Progeny 350 w	$199.99	1	$199.99
Sampling gear cost				$358.56
Essential Water Quality Gear				
YSI Prosolo meter, ODO probe, case, sl	Xylem, university price. We have used 1, now will use 2 for outside measurements	$1,995.60	2	$3,991.20
BOAT GEAR				
davit with block		$400.00	1	$400.00
winch		$65.00	1	$65.00
anchors	for 3 point anchoring - 3 needed, 1 assumed with boat - 13 lb fluke anchor from Amazon	$99.99	2	$199.98
Boat gear total				$664.98
EXTRA GEAR (optional)				
Go Pro Black 7		$228.04	1	$228.04
Underwater light	Amazon, Suptig dive light 84 LED	$36.99	1	$36.99
Extras Total				$265.03
Labor				
		Per hour		
Machine Shop	Per hour, billing in progress, best estimate	$75.00	15	$1,125.00

Appendix II. Cost Estimates For Denitrification

Unit Costs of Denitrification

Estimating a cost of each measurement of denitrification has a series of considerations:

1. Mobilization costs are a major consideration. We would anticipate that at least 4 individual measurements could be made in on day – with 4 deployments of the lander. Up to 6 may be possible, but could not be promised.
2. We use costs for two senior scientists to operate the lander, with some preparation time for a lab assistant to label vials. Costs are likely much lower.
3. We use boat costs for the Horn Point Laboratory.
4. Analytical costs are based on labor plus mass spectrometer rental for gas analysis, plus the current cost to HPL for analysis at the CBL analytical services. Within the Cornwell laboratory, we can do the analysis for (much) less.
5. Our comparison to the tray approach has many assumptions about personnel costs. HPL does not have diving capability and we assume $1,000 per day for a diver, which may be low.
6. We assume all gear is good for 25 days of deployment. This is likely lead to a high number, especially since the gear may last much longer. However, personnel and analytical costs are largest.

The lander measurement costs are better constrained; the tray approach utilized diving resources that are no longer available to us (i.e. VIMS personnel under the supervision of Dr. Lisa Kellogg).

Table 3. Cost comparison, lander versus tray approach. The spreadsheet (CBT Cost Comparison.xlsx) shows the costs in great detail.

Cost Category	Lander – This Study	Tray Approach Kellogg et al. 2013
Personnel	812	1,832
Boats & Logistics	79	164
Analytical	671	407
Gear (amortized - 25 deployments)	54	75
Per Measurement	1,615	2,477
With 26% overhead (State of MD)	2,035	3,121
With 55 % overhead (Federal)	2,503	3,839

There some efficiencies available for the lander approach. Replacing Cornwell with a junior scientist would result in a saving of ~$101 per measurement (before overhead). If the laboratory has the equipment, the nutrient analysis costs could be decreased substantially and the sample analyzed more rapidly (i.e. with getting into a busy sample stream elsewhere). For the lander, personnel costs were ½

of the total cost and for the tray approach, they were ~3/4 of the cost. It is possible that up to 6 incubations could be done in a day if 1) rates were high, 2) logistics was easy, and 3) the weather was cooperative.

For a broader cost comparison, these numbers compare favorably with costs for sediment incubation. Benthic flux measurements at CBL, utilizing large vessel, were $3,500 >10 years ago. Work in mesocosms in Florida cost $1,300 per core, with minimal sampling logistics and incubation of 20 cores per day (Cornwell et al. 2019).

Lander (4)												**Hours**				
Personnel		**Daily Rate**										**Scientist 1**	**Scientist 2**	**Res Assist**	**Diver 1**	**Diver 2**
	Senior Scientist 1	**$1,130.00**						**Labor**	**Preparation Day Before**				**4**	**2**		
	Senior Scientist 2	**$689.00**							**Field Day**			**8**	**8**			
	Research Assistant	**$215.00**							**Gear Cleanup**				**2**			
									Calculations				**8**			
		Benefits														
									Total	**Hours**		**8**	**22**	**2**		
Boat	**Daily Rate**			**230**	**1**	**$230**				**Days**		**1**	**2.75**	**0.25**		
	Boat Fuel (< 10 gallons)			**45**	**1**	**$45**										
	Truck (< 50 mile round trip)			**75**	**1**	**$75**				**Cost**		**$1,130.00**	**$2,062.50**	**$53.75**		
				Sum		**$350**										
										Total		**$3,246.25**				
Chemical Analysis		**#**	**Unit cost**													
	Dissolved gas samples	**36**	**12**	**432**								**Scientist 1**	**Scientist 2**	**Res Assist**	**Diver**	**Diver**
	Ammonium analyses	**36**	**9.82**	**353.52**						**Daily Rate**		**1130**	**750**	**215**	**1000**	**1000**
	Nitrate+Nitrite analyses	**36**	**9.82**	**353.52**												
	Soluble reactive phosphorus	**36**	**9.82**	**353.52**												
	Bromide analysis	**40**	**29.75**	**1190**												
Total analytical				**2682.56**												
Total Cost	**Personnel**	**$3,246.25**														
	Boats & Logistics	**$350.00**														
	Analytical	**$2,682.56**														
	Gear (amortized - 25 days of measurements)	**$217.41**														
	Total	**$6,496.22**														
	Per Measurement	**$1,624.06**														

Trays (8)																
Personnel		Daily Rate										Scientist 1	Scientist 2	Res Assist	Diver 1	Diver 2
	Senior Scientist 1	1130						Labor								
	Senior Scientist 2	629							Tray Deployment			16	16		8	8
	Research Assistants	215							Prep For Fluxes				8	2		
									Tray Recovery			16	16		8	8
		Benefits							Incubation			16	16	16		
					Days	Sum			Gear Cleanup				2	8		
Boat	Daily Rate			230	4	920			Calculations				16			
	Boat Fuel (< 10 gallons)			45	2	90										
	Truck (< 50 mile round trip)			75	4	300										
				Sum		1310										
Chemical Analysis		#	Unit cost													
	Dissolved gas samples	72	12	864												
	Ammonium analyses	72	9.82	707.04												
	Nitrate+Nitrite analyses	72	9.82	707.04												
	Soluble reactive phosphorus	72	9.82	707.04								Scientist 1	Scientist 2	Res Assist	Diver	Diver
	Bromide analysis	9	29.75	267.75						Daily Rate		1130	750	215	1000	1000
Total analytical				3252.87												
									Total	Hours		32	58	26	8	8
Total Cost	Personnel	$14,656.25								Days		4	7.25	3.25	2	2
	Boats & Logistics	$1,310.00														
	Analytical	$3,252.87								Cost		4520	5437.5	698.75	2000	2000
	Gear (amortized - 25 deployments)	$600.00														
	Total	$19,819.12								Total		14656.25				
	Per Measurement	$2,477.39														